



KTH Engineering Sciences

Alternative approaches to rear end drag reduction

Technical Report

Torbjörn Gustavsson

Stockholm 2006

KTH, Department of Aeronautical and Vehicle Engineering
Royal Institute of Technology

TRITA-AVE 2006:12
ISSN 1651-7660

www.kth.se

Preface

This paper was originally formed during my stay at KTH Startupfactory in the autumn of 2003. The intent of that stay was originally to make a commercial product out of the patent I received the same year. The project turned into research and one result is this paper.

For further inquiries in the area I can be reached by e-mail: torbjorn@vortaflow.com

Sincerely yours

Torbjörn Gustavsson

www.vortaflow.com

Reaching for the stars...

Acknowledgements

Above all I would like to thank Kim Noura for his support during my stay at KTH Startupfactory.

Second I would like to thank all my friends and family, especially my brother and mother, for support and feedback during development of this project.

I also would like to thank John C Lin at NASA Langley Research Centre who is the source of many of the reports I used as reference material. He has produced an amazing amount of work in very interesting areas and I also would like to thank him for providing some of his material free of charge. Hopefully I will get the opportunity to meet him some day.

Last but not least I would like to thank Tomas Melin and Arthur Rizzi at the Department of Aerodynamics at KTH for supporting the idea that the subject I buried myself so deep in could end up in something else than just knowledge, that is this report. Without them this work would never have taken place.

Abstract

This report begins with a short introduction to the problem of aerodynamic drag for commercial vehicles.

The main subject is a survey of different technologies available for decreasing drag and increasing performance on blunt bodies and diffusers. Initially the work done by NASA on the area of boat-tailing a bus is overviewed. After that the focus turns to the Coanda-effect and the possibility to use it to improve performance on trailers in the areas of fuel consumption, braking and dynamic stability. Boat-tail plates finish up the studies performed on commercial road vehicles.

The interests then turn to alternative, unconventional approaches to reattach flow over a backward facing ramp. Here are the use of primarily grooves and vortex generators surveyed. The report ends with a closer look on the use of micro vortex generators on a C-130 aircraft and the drag reduction created.

Table of Contents

- 1.NOMENCLATURE AND ABBREVIATIONS..... 6**
- 2.INTRODUCTION..... 7**
- 3.DIFFERENT TECHNOLOGIES..... 8**
 - 3.1. BOAT-TAILING..... 8
 - 3.1.1. *Controlled boundary layers* 12
 - 3.1.2. *Aerodynamic boat-tail*..... 23
 - 3.2. GROOVES..... 27
 - 3.2.1. *Transverse and swept grooves*..... 28
 - 3.2.2. *Longitudinal grooves*..... 32
 - 3.2.3. *Passive porous surface*..... 33
 - 3.3. VORTEX GENERATORS..... 34
 - 3.3.1. *Vane-type vortex generators*..... 34
 - 3.3.2. *Wheeler vortex generators*..... 35
 - 3.3.3. *Blunt body application of Vortex Generators*..... 41
- 4.CONTINUED WORK..... 46**
- 5.CONCLUSIONS.....47**
- 6.REFERENCES..... 49**

1. Nomenclature and abbreviations

3D	three dimensional
α	angle of attack in degrees
β	angle toward freestream flow
δ	boundary layer thickness
λ	spanwise distance between each geometric cycle
Δ	difference
Δp^*	drop of piezometric pressure over length l_1
ρ	air density
a	groove depth
b	groove spacing
C_d	drag coefficient = $F_D/(\rho \cdot U^2 \cdot /2)$
C_μ	momentum coefficient = $(m \cdot V_j)/(q \cdot S_{ref})$
CFD	Computer Fluid Dynamics
d	VG spacing
d_p	pipe diameter
D_h	horizontal offset of boat-tail plates divided by the width of the trailer
D_v	vertical offset of boat-tail plates divided by the width of the trailer
e/h	non-dimensional device length
f	friction factor, roughness and Reynolds number dependent
GTRI	Georgia Tech Research Institute
h	VG height
l	VG length
l_1	pipe length
L_p	boat-tail plate length divided by the width of the trailer
m	air mass flow
P	air pressure
q	freestream dynamic pressure
Re	Reynolds number
S_{ref}	reference-/front- area
\bar{u}	mean velocity
U	free stream velocity [m/s]
V_j	isentropic airjet velocity
VG	vortex generator
w	truck width
x	distance

2. Introduction

Aerodynamic drag of a commercial vehicle is a large part of the vehicles fuel consumption, according to Hucho [1] it can contribute to as much as 60 % of the vehicles fuel consumption.

So far aerodynamic design of commercial vehicles has concentrated on the front end of the vehicle. Since it produces most drag it has been the most urgent part to optimise. This optimisation can easily be spotted on trucks and tourist coaches. The rear end configuration has up until recently been neglected. Gilhaus [2] acknowledge the fact that on tourist coaches the rear end can contribute to as much as 27 % of the over all drag. This is the reason to why the author has chosen to take a closer look at the different technologies available to reduce rear end drag. Much of this technology has its offspring in aeroplane aerodynamics and the design of diffusers.

The main focus will be on tourist coaches since they have a high average speed of operation and thus are more affected by the aerodynamic drag. All results given below can of course be applied to all kind of vehicles such as trucks and otherwise blunt vehicles moving with high average speed. But the authors experience is that the market for tourist coaches is more openminded.

3. Different technologies

3.1. Boat-tailing

The most common and natural way of reducing rear end drag is boat-tailing, also called rear end tapering. It offers a technology commonly known, widely used and with recognised effect. But the practical application of it is limited due to the fact that it greatly reduces the comfort for the passengers and loading capability, see figure 1. Taking tapering to its drag reduction possibility limits is not a realistic possibility of practical reasons but it is still interesting to study the results of such research since it could be used as a benchmark and goal for other studies.

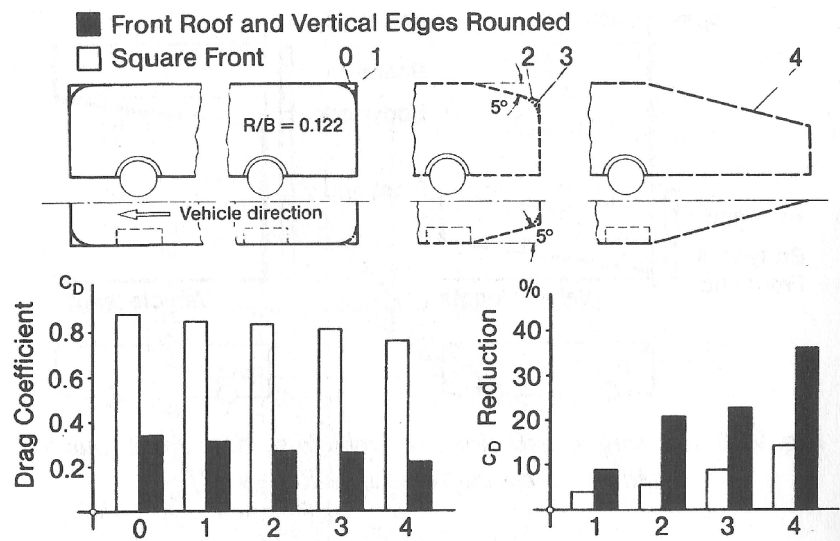


Figure 1: Effects of tapering the rear end of a tourist coach [1].

Nasa [3] performed a series of tests that suggest the use of a truncated boat-tail. With full-scale tests they achieved a drag coefficient of 0.302 with a full boat-tail (figure 2) and a drag coefficient of 0.307 with a truncated boat-tail (figure 3) this when a bus without a boat-tail has a C_d of 0.445. It can also be compared to a rounded nose section that according to Blevins [4] has C_d of approximately 0.6 when Reynolds number is $>10^4$.

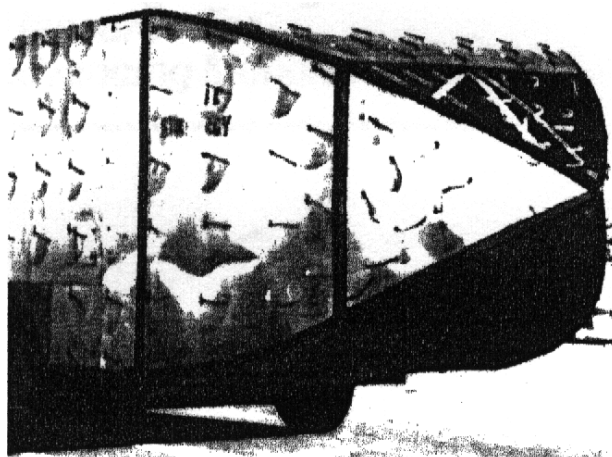


Figure 2: Full scale tests of a boat-tail at Nasa Dryden. [3]

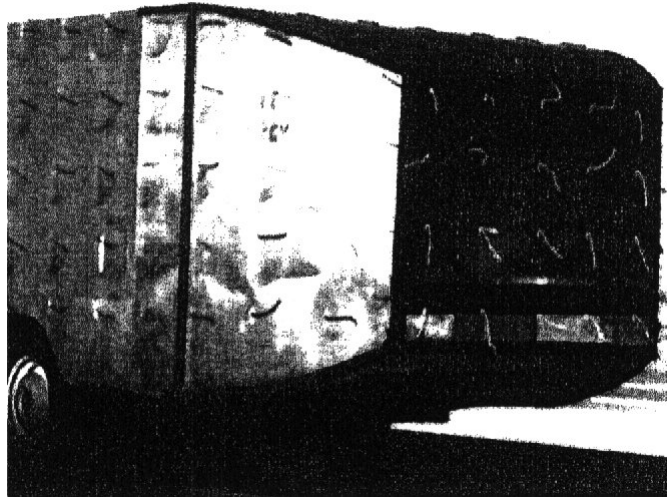


Figure 3: Full scale tests of a truncated boat-tail at Nasa Dryden. [3]

The truncation of the boat-tail was done at the natural point of separation. A less curved boat-tail would probably given larger differences between a full boat-tail with fully attached flow and a truncated boat-tail

Tests were performed at speeds ranging up to 26 m/s (93.6 km/h) and corresponding Reynolds number ranged up to $1.3 \cdot 10^7$. That includes the length of both the vehicle and the boat-tail. The general description of vehicle used in tests is described in figures 4 and 5.

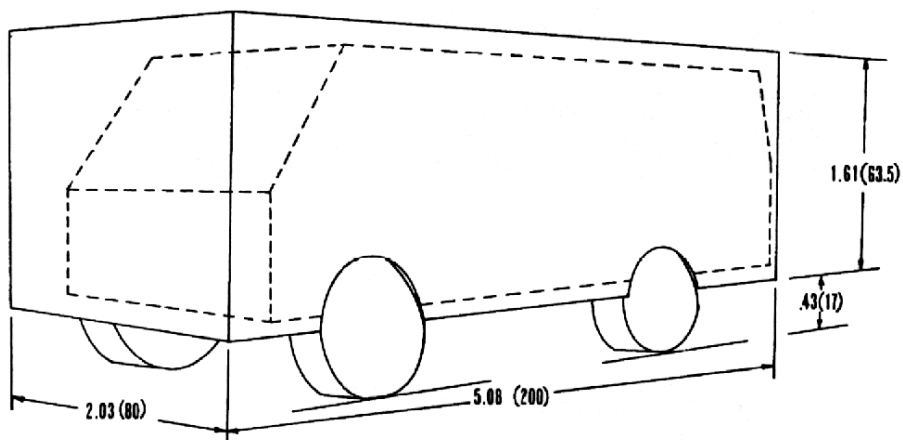


Figure 4: Dimensions of the original truck with squared corners in meters (inches). [5]

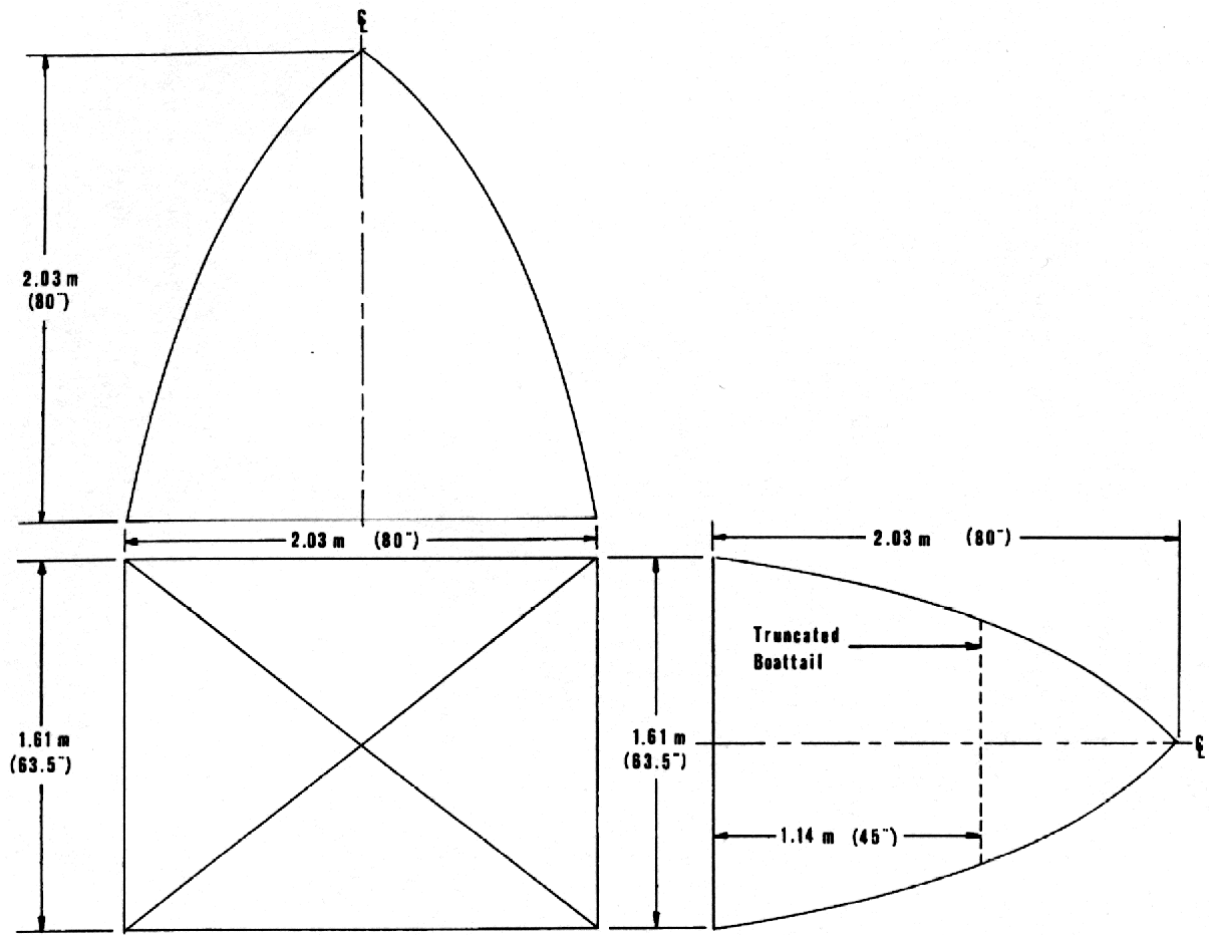


Figure 5: Dimensions of full and truncated boat-tail. [5]

Tests were performed with forebody, horizontal and vertical corners rounded and a faired and sealed underbody. This to avoid separation of airflow at the front end of the vehicle and to maximise the effect of the boat-tail configuration compared to no boat-tail.

The results of the test are compressed to figure 6 and they indicate that an average of 32 % drag reduction [5] was attained with the full boat-tail compared to a blunt rear end.

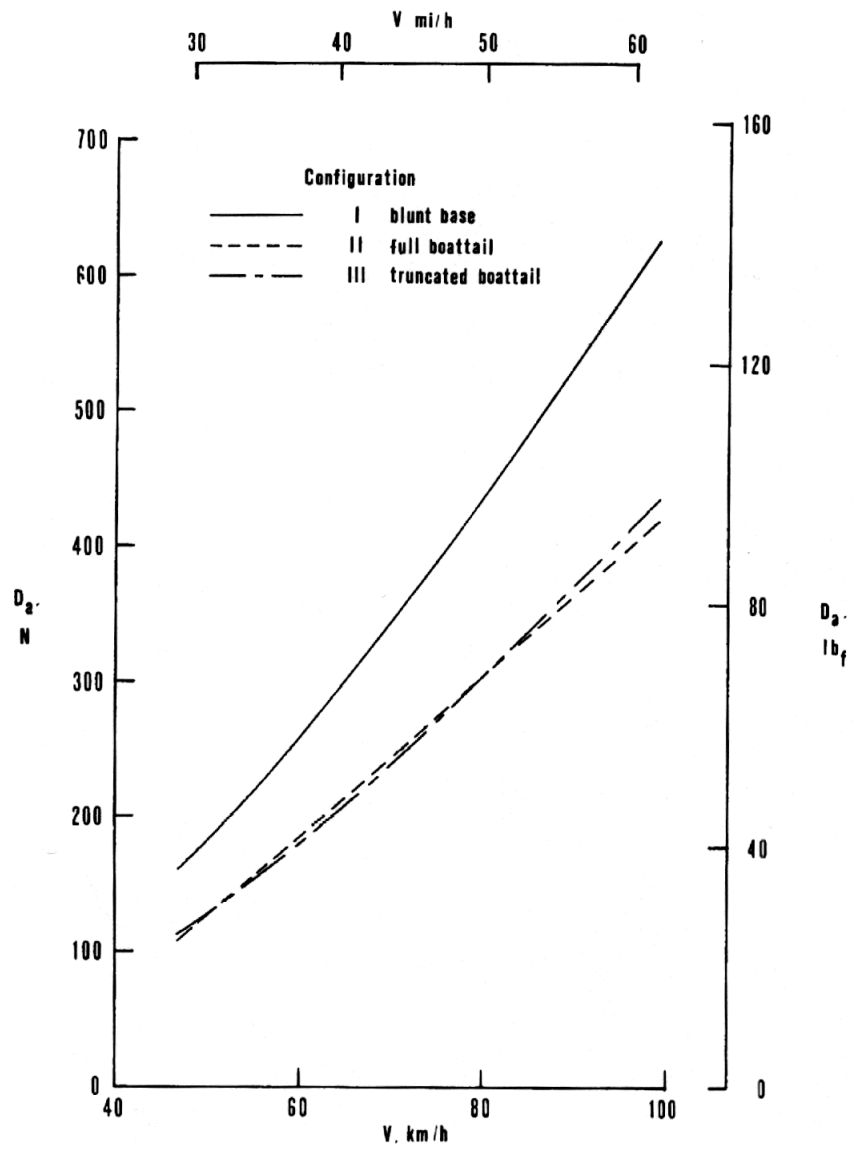


Figure 6: Aerodynamic drag versus vehicle velocity for different configurations tested at Nasa Dryden. [5]

3.1.1. Controlled boundary layers

Active separation control system of rear end flow can be performed with tangential blowing as suggested by Englar [6], [7] among others. The technology is also called the Coanda Effect named by Henri Coanda. The idea is that a slow airflow that generally would separate over a surface is energized with a high-velocity flow and thus the flow becomes attached to a curved surface as shown by figure 7.

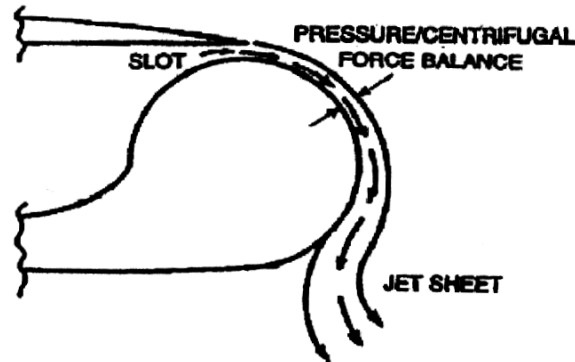


Figure 7: The Coanda effect demonstrated on a trailing edge. [6]

This can also be balanced with the possibility to suction of the boundary layer. These two technologies combined give the theoretical reduction of 40 % in aerodynamic power.

The trailer configuration simulated at Georgia Tech Research Institute (GTRI) is illustrated in figure 8. The main blowing slots are placed at each rear corners and one slot at the top leading edge to avoid separation at the front end of the trailer.

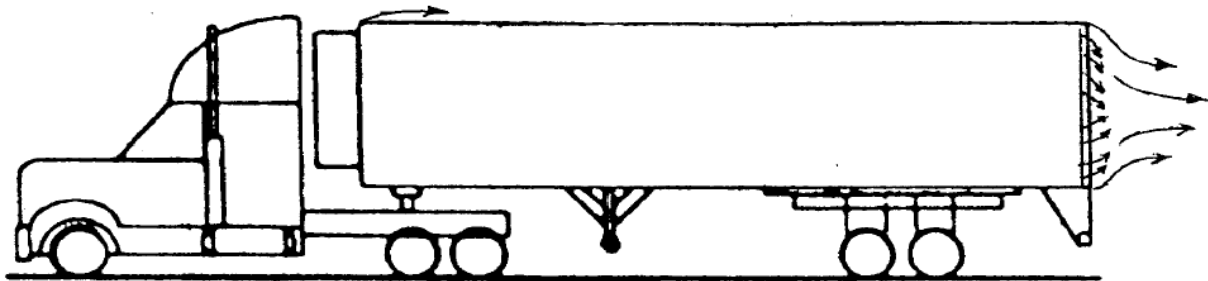


Figure 8: The trailer configuration simulated at the Georgia Tech Research Institute. [6]

Blowing all rear slots could reduce spray and drag and just blowing one slot at the rear control the aerodynamic side forces and thus give dynamic control to the vehicle. This could for instance be used to increase lift on the trailer and thus reduce rolling resistance and tire wear. In the opposite way it is possible to increase downforce on the trailer and provide braking assistance when needed and improve handling during slippery conditions. The effect of wind gusts could be controlled and managed with such a system and reduce the risk of jack-knifing.

As a source of airflow GTRI suggested a second turbo generator. This to reduce influence of engine performance that otherwise would be adverse using bleed of existing turbo pressure or engine exhausts directly.

Using a secondary turbo it is necessary to channel the air from the engine compartment to the rear of the trailer. In the case of a standard trailer we assume the length of 7 m for the trailer

and the thickness of the walls limit the diameter of the tubes from the extra turbo to the rear of the truck to a diameter of approximately 0.1 m. With housing from the extra turbo mounted on the trucks exhaust system it would give an overall length of the tubing of approximately 10 m.

By assuming airspeed of 30 m/s in the tubes and a friction factor of 0.0015 (fig 7.2 [8]) and using equation 7.1 from Massey [8] we get a pressure drop of:

$$\frac{\Delta p^*}{\rho \cdot g} = \frac{4 \cdot f \cdot l_1 \cdot u^{-2}}{d_p \cdot 2 \cdot g} \Rightarrow \Delta p^* = \frac{\rho \cdot 2 \cdot f \cdot l_1 \cdot u^{-2}}{d_p} = \frac{1,225 \cdot 2 \cdot 0,0015 \cdot 10 \cdot 30^2}{0,1} = 351 Pa \quad (1)$$

This does not include losses from couplings and bends and similar since the formula is used for “long, unobstructed, straight pipes” so the loss can be considered to be even higher. A lower airspeed reduces pressure loss. Another problem using bleeding of turbopressure is that the pressure might not be available when breaking and turning since the engine is running under low revs and not generating full pressure. A solution might be to add another tank of air under pressure generated by the compressor to guarantee airsupply under all conditions.

For wind-tunnel tests GTRI used a model described by figure 9.

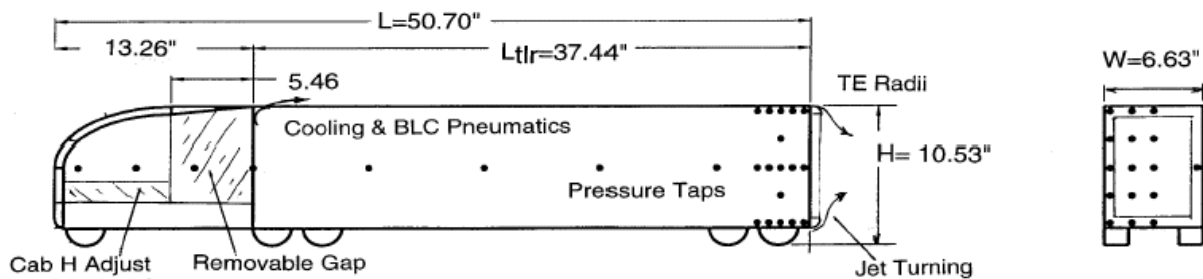


Figure 9: GTRI wind tunnel model is a generic description of a tractor-trailer configuration. [6]

The GTRI wind-tunnel model has a square section area of 0.83 m² (1290 sq. in.) and the size of the model is a 0.065-scale model of a truck that produced a 5.1 % wind-tunnel blockage. The Reynolds number based on trailer length was 1.9·10⁶ at U = 31 m/s (70 mph) or 3.9·10⁶ at tunnel maximum speed.

Figure 10 show the possibility in drag reduction for a 29.5-ton (65 000 pound) 18-wheel tractor-trailer rig with a frontal area of 10 m² (107.5 sq. ft.).

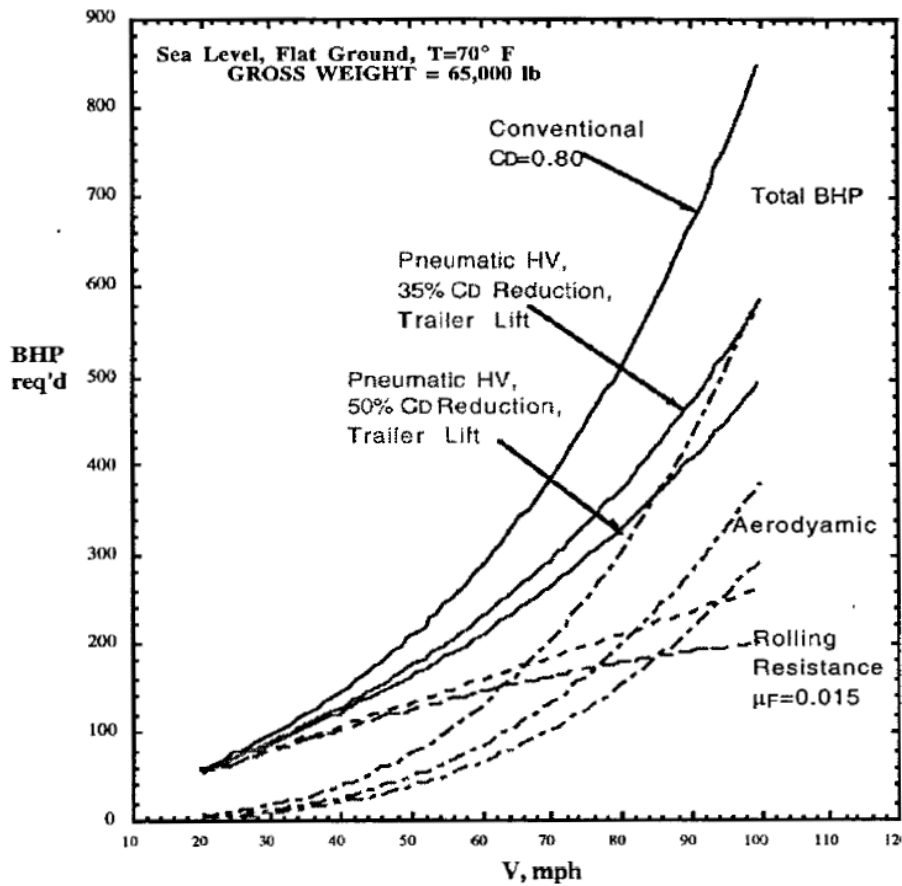


Figure 10: Drag reductions due to blown boundary layers as suggested by GTRI. The upper curves representing total horsepower required at the wheels to overcome all forces present. [6]

At a speed of 31 m/s (70 mph), power required to overcome drag and rolling resistance can be reduced by 24 respectively 32 % as suggested by Figure 10.

Navier-Stokes equation based Computational Fluid Dynamics analysis was performed at Georgia Tech School of Aerospace Engineering. Differences in predicted flow are presented in figures 11a and b.

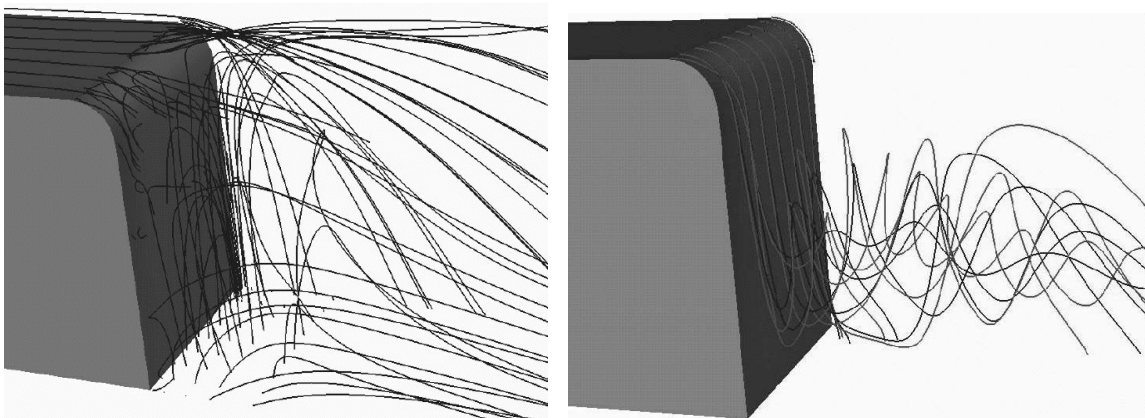


Figure 11(a-b): CFD predictions of unblown and blown boundary layer performed at Georgia Tech School of Aerospace Engineering. The reattachment of the flow clearly indicates the possibility to reduce base-drag of current configuration. [6]

GTRI manage to show through wind-tunnel test on the model described above that C_d is reduced by 8 % just by rounding the leading edge of the trailer. If the aft edges are rounded the drag reduction is of magnitude 7 % and that is without blowing of the boundary layer. These simple steps add up to a drag reduction of 15 % which clearly is a simple way to reduce fuel consumption. This is of course when fairing of the tractor-trailer gap is performed. Without closing of the gap between the tractor and the trailer the drag increases dramatically, especially in side-wind conditions.

As figure 12 depicts there can be major gains in blowing the trailing edges of a trailer. The benefits of the technology is of course at its best when performed on all four sides. The tests were performed at wind-tunnel speeds of 31 m/s (70 mph), dynamic pressure of 8 Pa (11.86 psf) and Reynolds number of $2.51 \cdot 10^6$ based on total length. At some conditions a 50 % drag reduction was measured when using blown boundary layers.

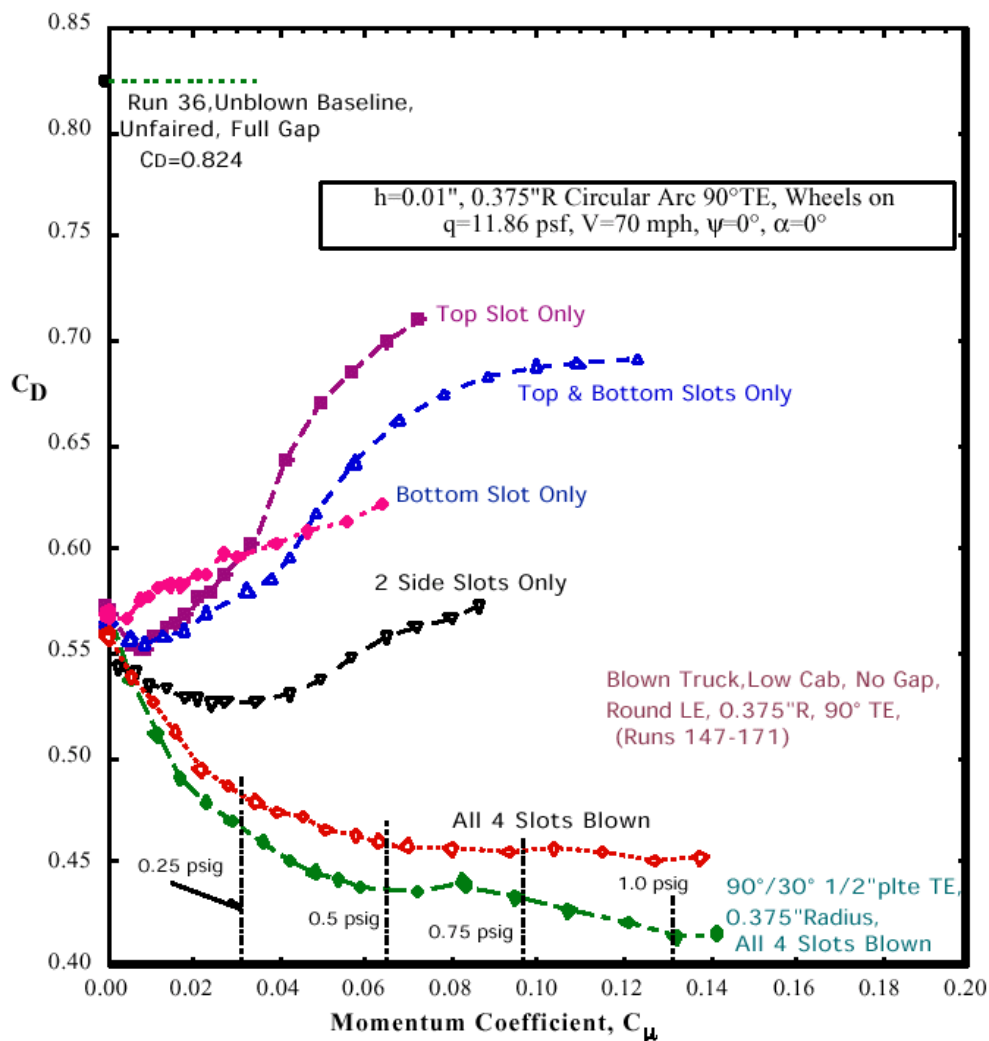


Figure 12: Drag reduction when blowing different rear trailing edges at tests performed at GTRI. [7]

During some specific conditions, blowing over top and bottom slot only, drag increased. This could be, as mentioned earlier, be useful when breaking the truck.

Some configurations with blown boundary layers and sealed fairing between tractor and trailer show such small values of C_d as some sports cars in the range of 0.3. This is then when the

tractor still is missing several "reality bits" such as engine cooling intake, mirrors, rough underbody and body component mounting mismatches. When all of these come into play we can expect C_d to rise to "normal" values once again. But it is an example of what the technology could be able to do in the future when more careful manufacturing methods and attention to details and aerodynamic drag is deployed.

Measurements of lift varied with different slot blowing configurations as can be seen in figure 13. These qualities can be used to decrease rolling resistance or increase wheel pressure to reduce braking distances.

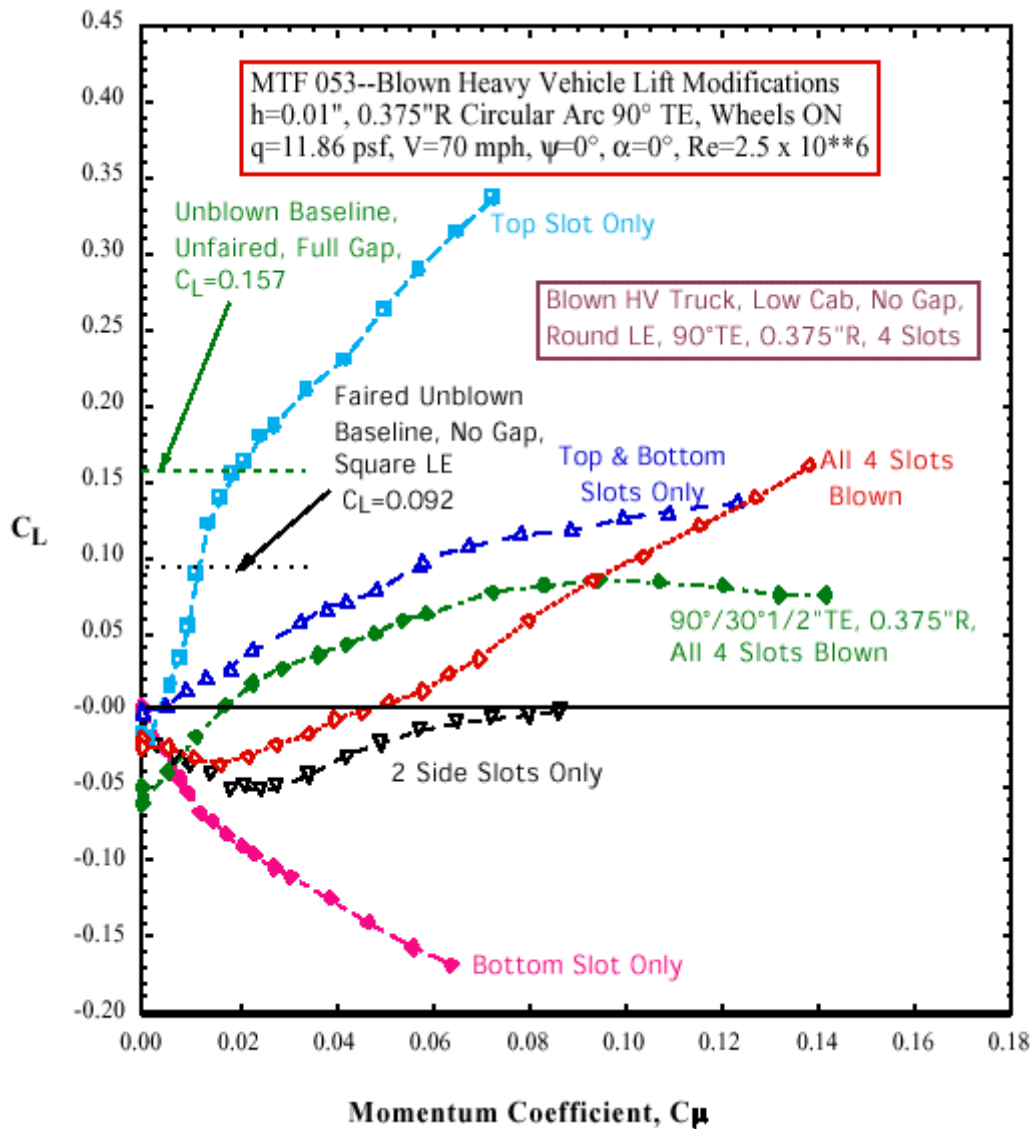


Figure 13: Tests at GTRI show that it is possible to use tangential blowing as a way to increase or decrease lift on the trailer. [7]

P. Ferraresi [9] performed in cooperation with Scania AB a series of CFD tests based on a simple truck model consisting of a prism with rounded edges and without wheels. Comparison was made with a wind-tunnel model based on the Peps configuration with the Volvo wind-tunnel as reference. The Peps configuration is an aerodynamical ideal truck-trailer combination with 5.3 m length, 1.3 m width and 2 m height.

At a simulated velocity of 44.4 m/s and a reference frontal area of 1.3 m², only half of the truck was modelled due to symmetry reasons, the results suggests a 29 % reduction in drag without blowing the boundary layers as table 2 show and the different configurations tested is shown in figure 14.

Truck configuration	C _d	Reduction
Basic	0.326	
Boat-tail, l _t = 0.5, φ = 15°	0.23	29 %
Boat-tail, l _t = 0.25, φ = 15°	0.271	17 %
Boat-tail, l _t = 0.1, φ = 15°	0.285	12 %
Round, radius = 0.1 m	0.293	10 %
Round, radius = 0.2 m	0.28	14 %

Table 1: Result for CFD calculations at KTH. Reductions in drag are clear and this is without blowing of the boundary layers where l_t= tail length [m] and φ =tail angle. [9]

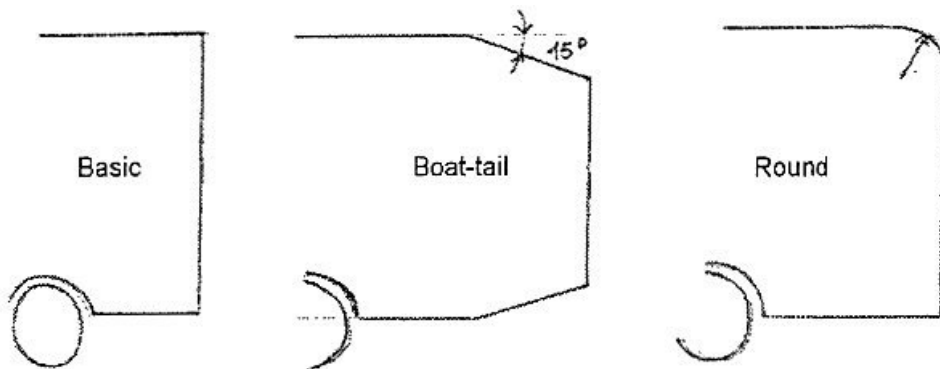


Figure 14: Different configurations simulated at KTH. [9]

Figure 15 present a reduction in drag for the rounded section as the radius increase.

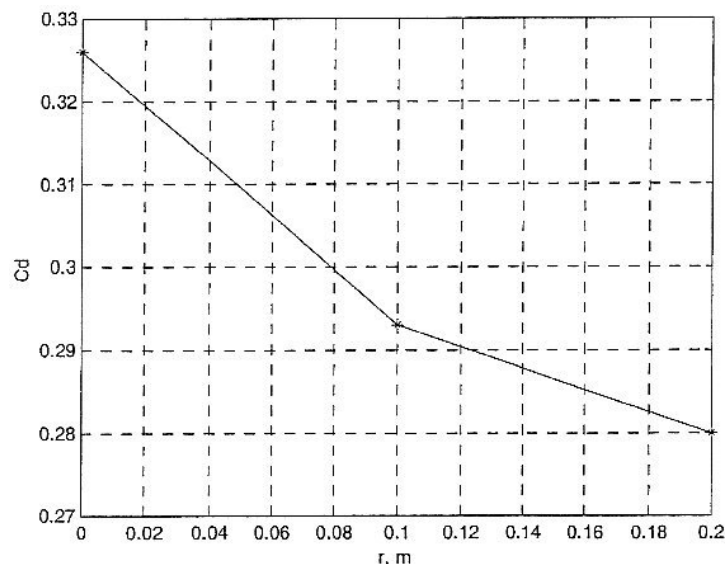


Figure 15: C_d versus rear end rounding radius. [9]

Further simulations were done with blowing of the boundary layer. The results are presented in table 2 and suggest a drag reduction of 29 % for boat-tail configuration and 17 % drag reduction for a rounded rear end configuration.

Configuration			C_d
Basic			0.326
Boat-tail	Length = 0.1 m	Basic	0.285
		Blowing	0.287, U = 0.4 m/s 0.275, U = 0.004 m/s
	Length = 0.25 m	Basic	0.271
		Blowing	0.291, U = 2 m/s 0.338, U = 33 m/s
	Length = 0.5 m	Basic	0.23
		Blowing	0.25, U = 0.4 m/s
Round	Radius = 0.1 m	Basic	0.293
		Blowing upper	0.278, U = 0.04 m/s
		Blowing upper + lateral	0.27, U = 0.04 m/s
		Punctual Blowing	0.28, U = 0.04 m/s
	Radius = 0.2 m	Basic	0.28
		Blowing	0.27, U = 0.04 m/s

Table 2: Result for CFD calculations at KTH when blowing the boundary layers. [9]

As before a long boat-tail proves to be the best configuration but the most interesting fact is that drag increase when blowing the boundary layer for that configuration. Suction was also tested and the results are presented in table 3 with a decrease of C_d of 29 % for boat-tail with length of 0.5 m and 24 % for a rear radius of 0.1 m.

Configuration			C_d
Basic			0.326
Boat-tail	Length = 0.1 m	Basic	0.285
		Suction	0.283
	Length = 0.25 m	Basic	0.271
		Suction	0.27
	Length = 0.5 m	Basic	0.23
		Suction	0.23
Round	Radius = 0.1 m	Basic	0.293
		Suction upper	0.27, U = 0.04 m/s
		Suction upper + lateral	0.247, P = -2500 Pa Average
		Points	0.27, P = -2500 Pa
	Radius = 0.2 m	Basic	0.28
		Suction upper	0.27, U = 0.04 m/s 0.265, P = -2200 Pa

Table 3: Result for CFD calculations at KTH when suction is applied to the boundary layer. [9]

The effects on the boat-tail (compared to no blowing or suction) is as before very small and will probably be balanced out by the energy required to propel any device for suction or blowing of the boundary layer. For the rounded trailing edges blowing and suction provide a

clear difference in performance. Since rounding of the edges is more beneficial considering spacing for passengers and load (cargo) it might be interesting to further investigate this technique.

Benjamin Le Roux [10] performed a series of half-scale tests at the MIRA wind-tunnel in England. The tests were performed on the PEPS half-scale model at air speeds of 28.4 m/s due to structural limitations of the model. The measurements of the model is:

- Length = 5.3 m
- Width = 1.3 m
- Height = 2 m

That give a reference (frontal) area of $S_{ref} = 2.4 \text{ m}^2$.

The overall configuration of the model is presented in figure 16 where the air intake, pump and jet device in pointed out. Scale is not respected in the drawing but should be considered a schematic. The jet device is closer described in figure 17.

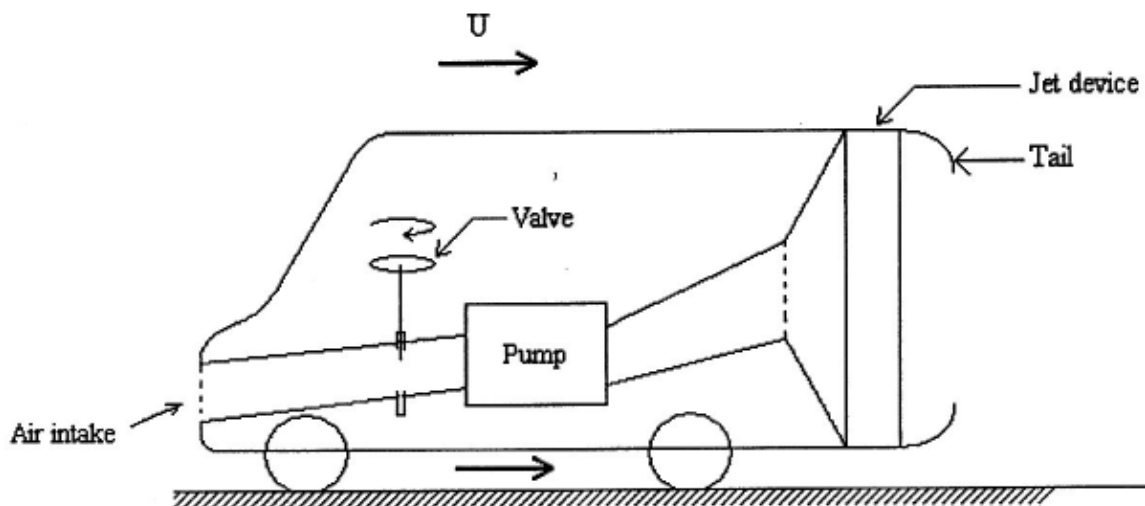


Figure 16: Overall view of the test model PEPS. [10]

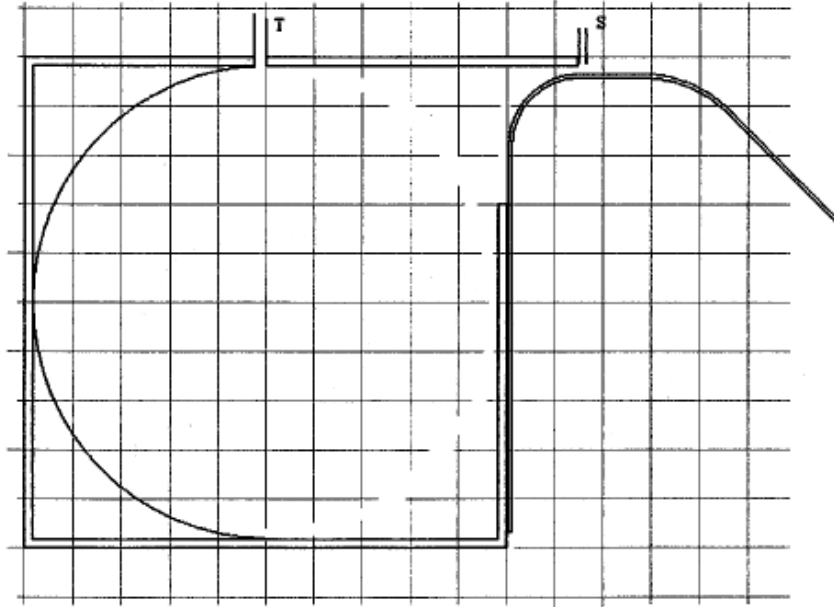
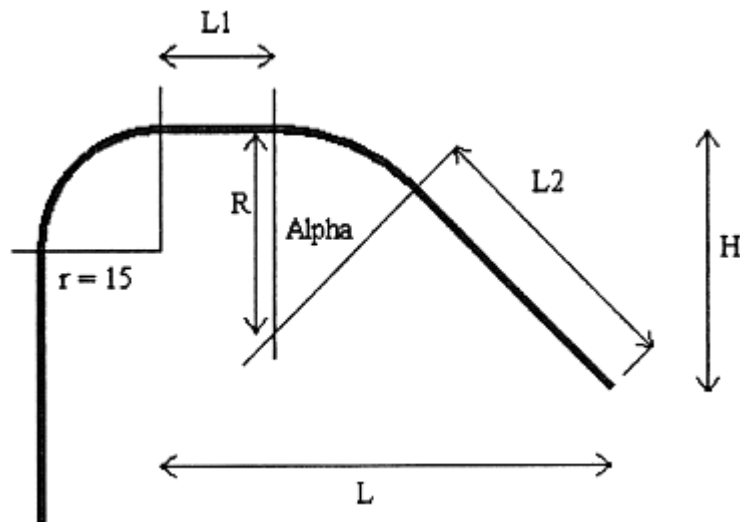


Figure 17: Jet device's section with a tail and pressure taps. [10]

The jet device cover the circumference of the aft of the truck and the air outlet is just below the “S” in figure 17. This gives the tangential blowing that is investigated. In order to maintain a steady flow the volume before the outlet is large and work as a plenum to equal out differences in pressure.

The tail section is defined by figure 18 and their variations during the tests are accounted for in table 4.



Figur 18: Tail section. L_1 - Flat extension of the trailer to study the effect of the location of the jet from the turning surface. R - Radius of the rounded part. α - Angle of the rounded part. L_2 - Flat part as a boat-tail. [10]

Name	Description	L_1 [mm]	R [mm]	α [°]	L_2 [mm]	L [mm]	H [mm]
T 1	Rounded	0	50	90	0	50	50
T 2	Rounded	0	100	90	0	100	100
T 3	Rounded	0	200	90	0	200	200
T 4	Rounded	0	300	90	0	300	300
T 5	Rounded	0	200	60	0	173	100
T 6	Mixed	0	200	60	200	273	273
T 7	Boattail	0	0	15	250	241	65
T 8	Boattail	0	0	20	250	235	86
T 9	Boattail	0	0	30	250	217	125
T 10	Mixed	50	0	30	250	267	125
T 11	Mixed	50	200	90	0	250	200
T 12	Mixed	100	200	90	0	300	200
T 13	Mixed	100	100	30	100	237	63
T 14	Mixed	100	100	45	100	241	100

Table 4: Variations of tail parameters during the MIRA tests. [10]

The length and height of the tail is given by formulas 2 and 3

$$L_{tail} = L_1 + R \cdot \sin(\alpha) + L_2 \cdot \cos(\alpha) \quad (2)$$

$$H_{tail} = R \cdot (1 - \cos(\alpha)) + L_2 \cdot \sin(\alpha) \quad (3)$$

The first aim of the experiments was to determine the best tail configurations. This was done using a 3 mm slot with blown and non-blown boundary layers to determine which configuration was most beneficial. Figure 18 show the different configurations tested and table 5 present the results.

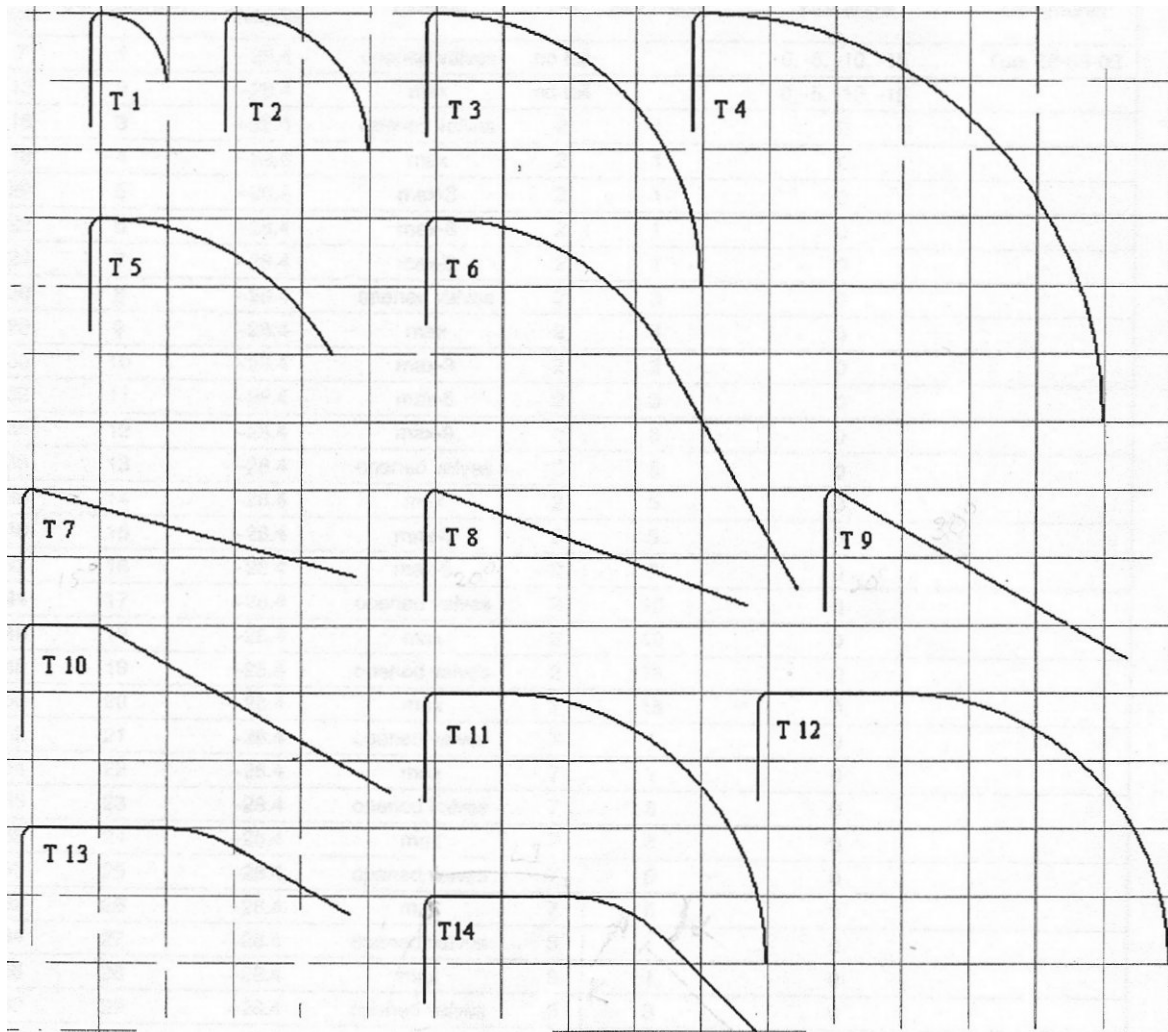


Figure 19: Different tail configurations tested at the MIRA wind-tunnel. [10]

<i>Name</i>	<i>Description</i>	<i>C_d without blowing</i>	<i>C_d with maximum blowing</i>	<i>ΔC_d [points] (positive for decreasing drag)</i>
Baseline		0,344	0,348	-4
T2	Rounded	0,347	0,338	9
T3	Rounded	0,346	0,339	7
T4	Rounded	0,340	0,340	0
T5	Rounded	0,341	0,332	9
T6	Mixed	0,345	0,346	-1
T7	Boat-tail	0,312	0,301	11
T8	Boat-tail	0,340	0,314	26
T9	Boat-tail	0,357	0,365	-8
T10	Mixed	0,359	0,348	11
T11	Mixed	0,344	0,342	2
T12	Mixed	0,343	0,347	-4
T13	Mixed	0,347	0,350	-3
T14	Mixed	0,345	0,352	-7

Table 5: Test results from MIRA with and without blowing of the boundary layers. [10]

It is clearly seen that configurations 7 and 8 are those who present the lowest drag and largest difference in C_d . Comparison between the tails 3, 11 and 12 shows that increased length of L_1 is not beneficial for drag reduction.

Tail number 5 show that there is no point in extending the tail beyond the point of separation, on the contrary, a prolonged tail beyond that point increase drag. So it would be interesting to find the point of separation and thus optimise tail length. But all these values are low compared to the ones achieved when using boat-tails and that configuration is to prefer.

The most beneficial configuration would be the 15° tail as confirmed by other tests at other times and as is shown by table 5. Further investigation of tail 8 was done since it in an early stage showed the highest drag drop. Different blow ratios and slot heights were tested and the slot height of 1 mm seems to be the most efficient. This might not directly be transferred to a full-scale model so in that case optimal slot height must be found.

The power savings on this devise was about 20 % compared to the reference values and was achieved as earlier mentioned with tail 8 and maximum blowing.

3.1.2. Aerodynamic boat-tail

An aerodynamic boat-tail, also called boat-tail plates, was evaluated at Nasa Ames Research Centre [11]. The configuration is described by figure 20. The idea is to trap a vortex or eddy in the corner between the rear of the trailer and boat-tail plates. The dimensions of the truck is not given in the report [11] but is assumed to be of standard dimensions.

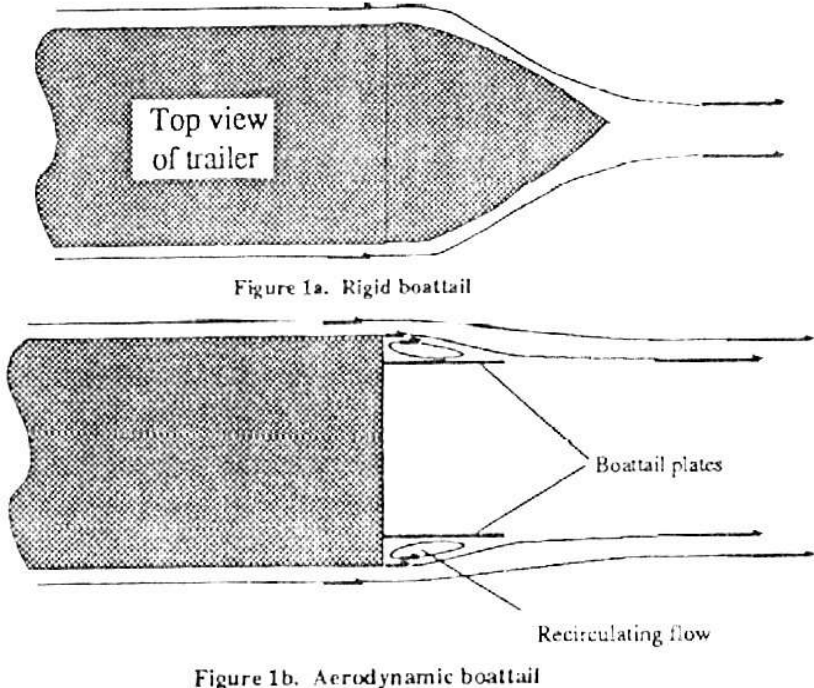


Figure 20: The configuration of aerodynamic boat-tail compared to ordinary rigid boat-tail. [11]

The eddy turn the flow inwards as it separates from the rear of the trailer and creates a virtual boat-tail and thus increase the base pressure acting on the rear of the vehicle and reduce the

net aerodynamic drag of the vehicle. Figure 21 show the aerodynamic boat-tail mounted on the rear end of the truck.

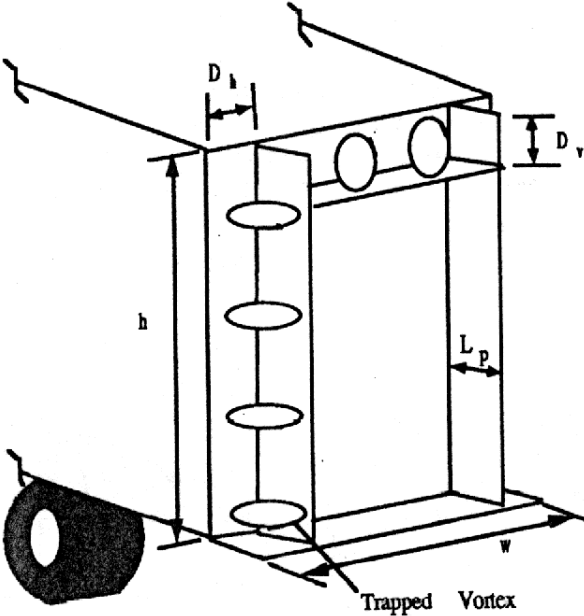


Figure 21: The rear end configuration of the trailer when performed wind-tunnel tests according to Lanser et. al. at the Nasa Ames Research Centre. [11]

Table 6 show the different geometrical configurations tested.

L_p	D_v	D_h
0.0	0,0	0,0
0.24	0.04	0,04
0,24	0.06	0.06
0.24	0.12	0.12
0.30	0.04	0,04
0.30	0,06	0.06
0.30	0,09	0.09
0.30	0.04	0.06
0,30	0.06	0.09
0.36	0.04	0,04
0.36	0,06	0,06
0.36	0.12	0.12
0.36	0.15	0.15
0.36	0.04	0,06
0.44	0.04	0.04
0.44	0.06	0.06
0.44	0.09	0.09

Table 6: Different configurations tested at the Nasa Ames Research Centre using the aerodynamic boat-tail described in Figure 21. All lengths and distances are normalised by the trailer width. [11]

In figure 22 a-b the pressure distribution across the rear doors of the truck at yaw angles 0 and $\pm 6^\circ$ are presented. It clearly shown (figure 22 b) that the pressure inside the aerodynamic boat-tail has increased. The maximal ΔC_d was received when horizontal and vertical offset (D_h, D_v) was $0.06w$ ($w =$ truck width) and $L_p = 0.36$.

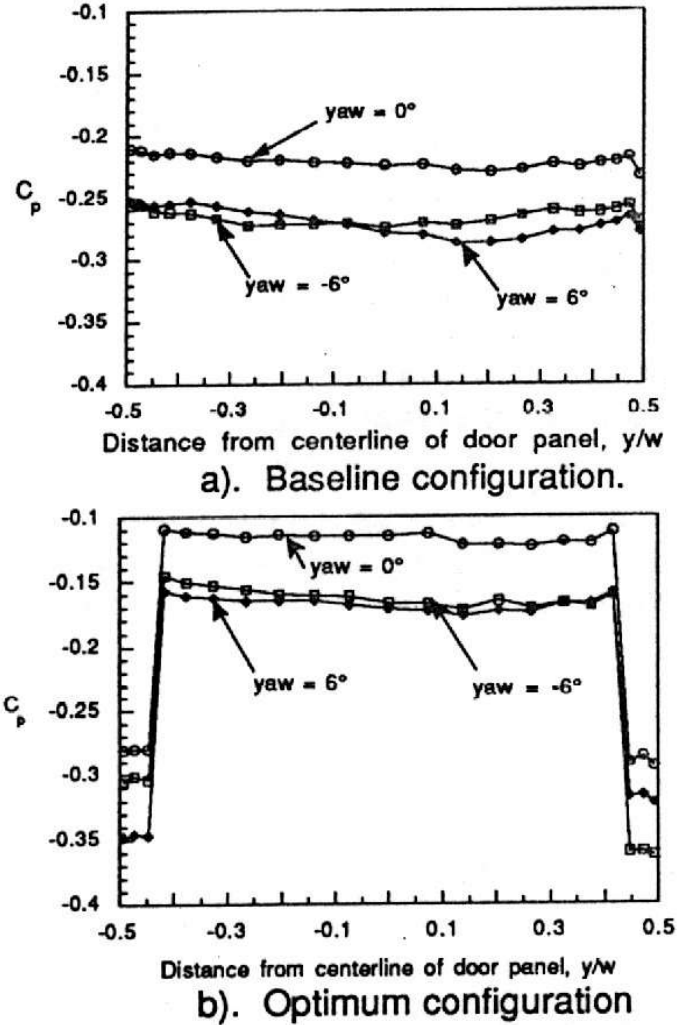


Figure 22(a-b): Pressure distribution over the centre of the rear doors for the baseline and optimum configuration. [11]

C_d data were obtained at a velocity of 25 m/s (58 miles/hour). The device consistently showed drag reductions in the range of 10 % but it was also sensitive to yaw angle as figure 23 show.

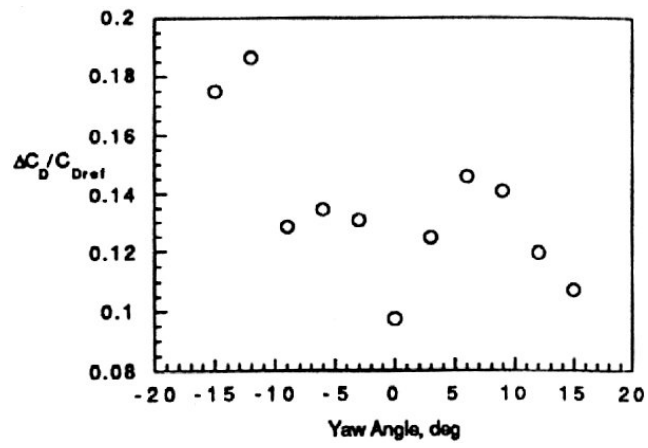


Figure 23: Change in drag as a function of yaw angle when optimum aerodynamic boat-tail is mounted. $C_{D,ref}$ is the original C_d of the truck with no aerodynamic devise mounted at the rear. [11]

3.2. Grooves

Another technology developed by J.C. Lin et. al. [12] but originating in the Soviet Union is the use of transverse and swept grooves. The work was performed on a diffuser but should be applicable on other areas too. Some 50 % drag reduction has been reported on bluff bodies with grooves.

J.C. Lin et. al. performed their tests at a Reynolds number of $5.1 \cdot 10^6$ at NASA Langley 51 x 71 cm tunnel, that is a low-turbulence, subsonic, open-circuit tunnel. Tests were performed at free-stream velocity of 40.2 m/s. Figure 24 describes the test configuration used. A suction slot was installed in front of the test section to remove any upstream influence on the test section. The ceiling of the tunnel above the test section was adjusted in a way to ensure a zero pressure gradient.

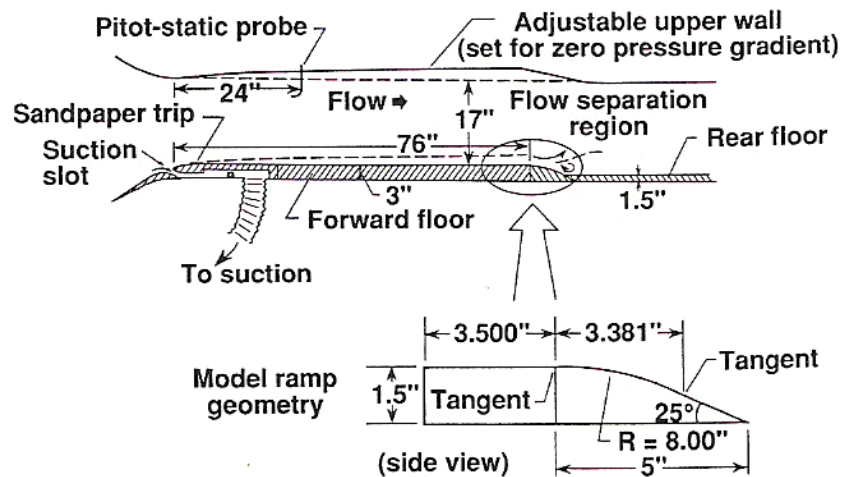


Figure 24: The test configuration at NASA Langley wind-tunnel performing test of grooves over a backward-facing ramp. [12]

The boundary layer just ahead of the separation ramp was fully turbulent and approximately 3.25 cm in thickness. The shoulder radius of the ramp was 20.3 cm (8 in.) and the ramp was at a 25° as shown by figure 24. The width of the test section was to full wind-tunnel width of 71 cm.

The flow separated at approximately the midpoint of the ramp without the grooves. The grooves were placed on the shoulder of the ramp and different geometries tested are presented in figure 25.

3.2.1. Transverse and swept grooves

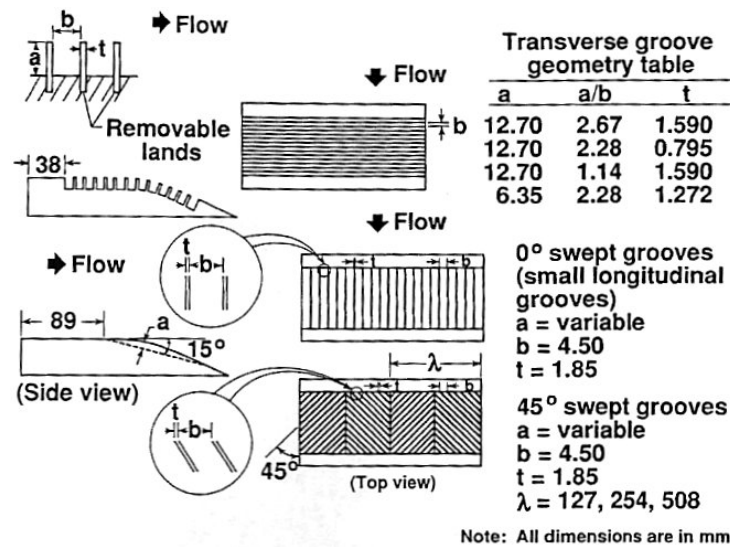


Figure 25: Different test geometry at NASA Langley wind-tunnel performing tests of grooves over a backward-facing ramp. [12]

Pressure taps registered the pressure distribution on the ramp and the floor downstream of the ramp. The results are presented in figure 26 and show acceleration and a symmetric deceleration when air flows around a corner; this is the reason for the pressure drop on the upstream portion of the shoulder.

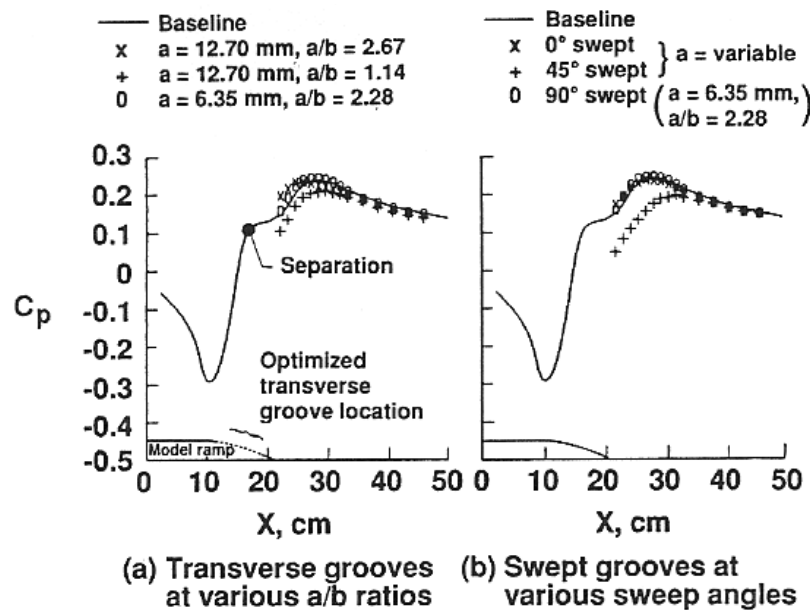


Figure 26: Pressure distribution of the backward-facing ramp. [12]

To illustrate flow separation oil flow was used. Some of the results are presented in figures 27 and 28.

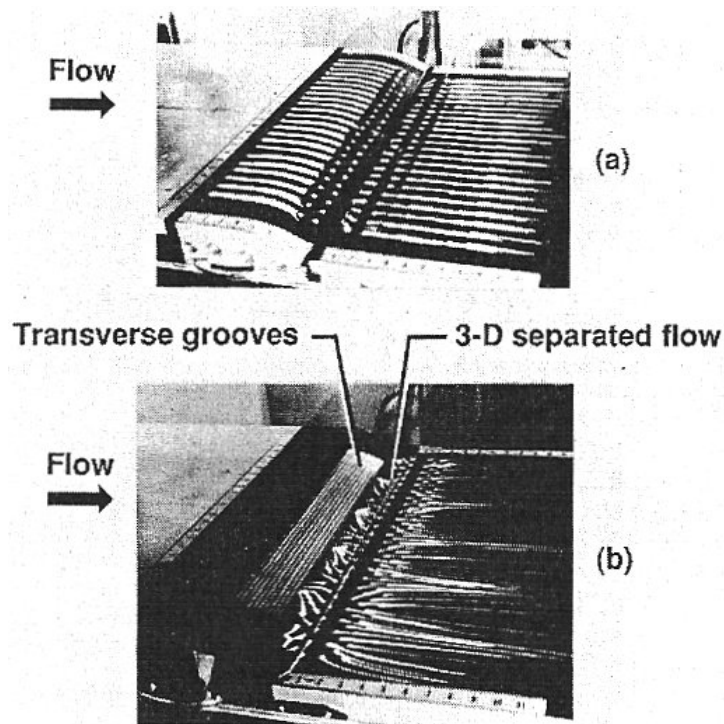


Figure 27: Oil flow over different ramp models were a) is the reference model and b) the model with transverse grooves. [12]

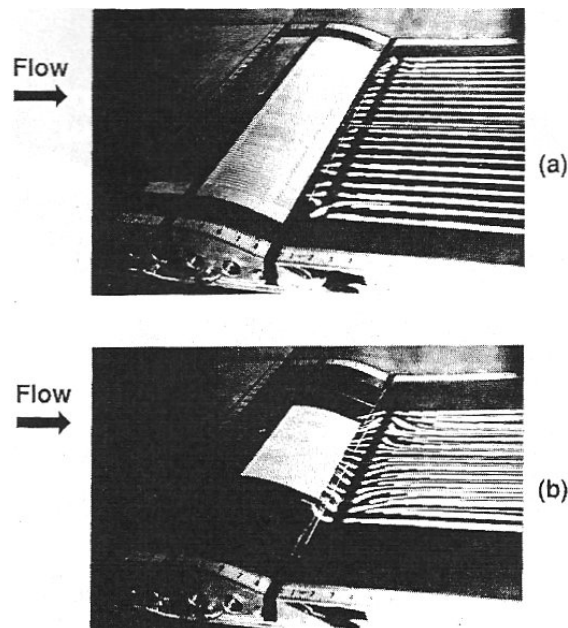


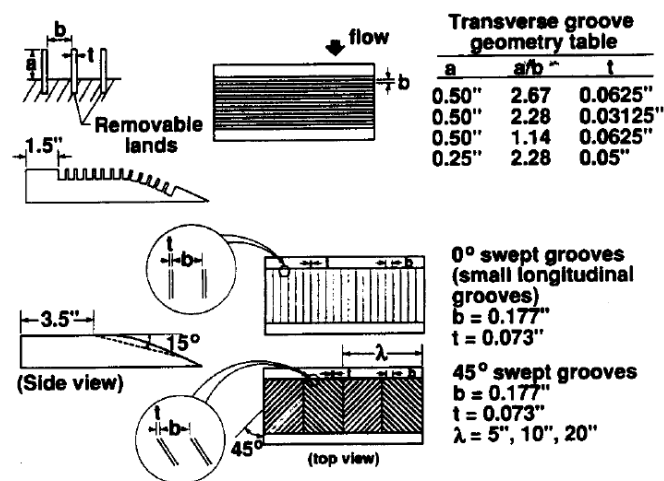
Figure 28: Oil flow over different ramp models where a) has longitudinal grooves and b) have 45 degree swept grooves. [12]

An optimum placement for transverse grooves proved to be to begin with the grooves one boundary-layer thickness upstream of the base model separation line and extending one boundary-layer thickness downstream of the separation line. This configuration reduced the distance from separation to reattachment by 20 %. The most effective configuration proved to have a depth-to-width ratio (a/b) of 2.67. Reduction of depth-to-width ratio reduced effectiveness of the device.

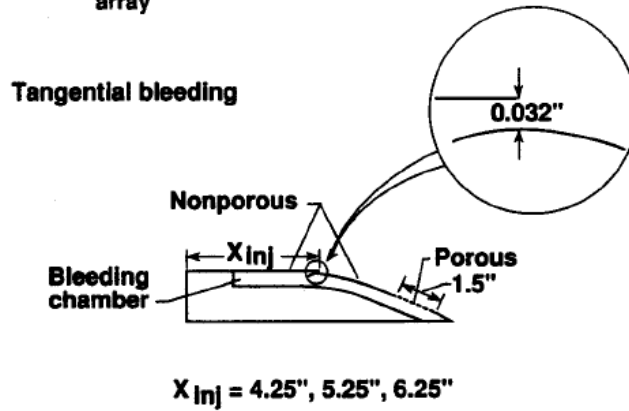
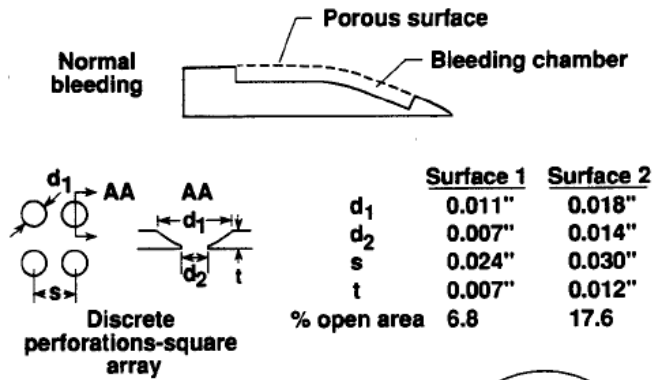
Using longitudinal and 45 degree swept grooves the depth (a) varied along each groove, from zero depth at the leading edge to about 0.64 cm at the midpoint. Since the pressure recovery (figure 26) is not as large using 45-degree grooves as using transverse we have an adverse result using the 45-degree grooves compared to baseline configuration. This could be explained by the same phenomenon as for transverse grooves with depth-to-width ratio of 1.14; the distance between the grooves is too small and the airflow experiences it as a closed cavity and thus there is no reduction in reattachment distance (the distance from reference separation line to maximum pressure coefficient).

The mechanism associated with different improvements in pressure recovery and reduction in reattachment distance is for the transverse grooves a “roller bearing” mechanism that can be explained in such way that the air rolls or rotates in each individual groove. For the longitudinal grooves it could be the technique of partial “boat-tailing”.

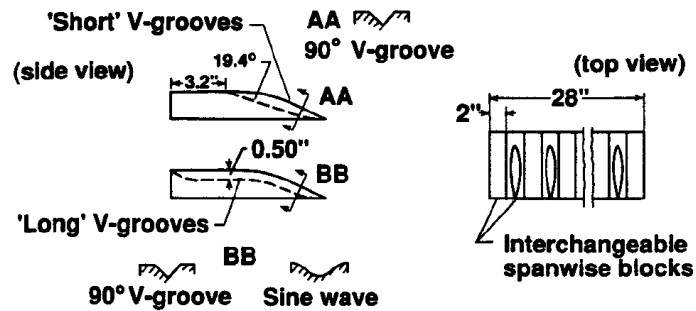
J. C. Lin et al [13] performed another series of tests that included many more different methods to improve pressure recovery on a backward facing ramp. The tests performed at NASA Langley [13] were performed at the same tunnel and same configuration as the tests with grooves described above [12]. The different test configurations are illustrated by figure 29 a-d.



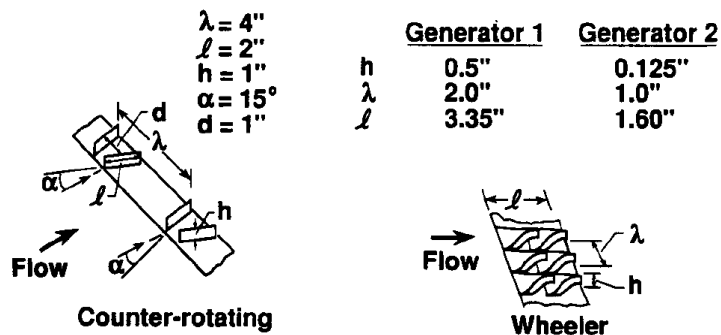
(a) Transverse and swept grooves.



(b) Passive porous surfaces.



(c) Longitudinal grooves.



(d) Vortex generators.

Figure 29 (a-d): Geometry of separation control devices. [13]

In contrary to what is said before [12] it is now stated [13] that a correct design of swept grooves probably will be more efficient than transversal grooves. That is founded on fact that there is a three-dimensional flow generated by the transversal grooves that is shown in figure 27 and this is what generate the beneficial flow. A proper design of swept grooves would reinforce this behaviour and possibly generate a reduction in reattachment distance.

Optimum transverse configuration described by figure 30, where $a/b = 2.67$, reduced the distance to reattachment by almost 50 %.

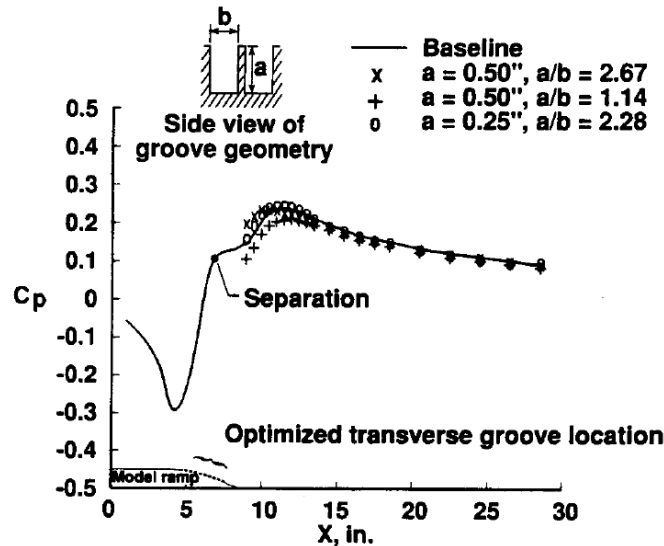


Figure 30: Pressure distributions for transverse grooves. [13]

3.2.2. Longitudinal grooves

Figure 29 c show the different longitudinal grooves that were tested. Figures 31 show the pressure distribution using the different grooves.

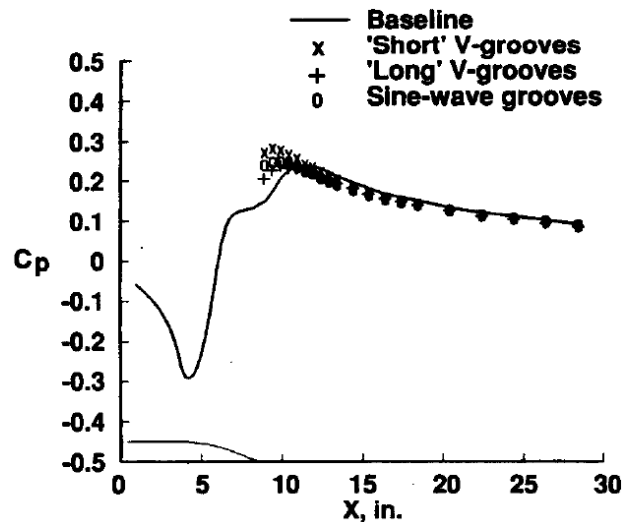


Figure 31: Pressure distribution for longitudinal grooves with 2-inch spacing. [13]

A separation of 50,8 mm (2 inches) between each groove proved to be most efficient spacing that were tested; it significantly reduced the distance to reattachment. As figure 31 show the

short V-grooves proved to be the most efficient configuration under these tests and it reduced the reattachment distance by 66 %. Worth mentioning can be that ‘short’-, ‘long’- and sine-wave grooves had a shorter reattachment distance than the smaller zero-sweep angle longitudinal grooves mentioned earlier [12]. For a 100 mm (4 inch) distance between the grooves the sine-wave configuration proved to be more efficient.

3.2.3. Passive porous surface

This technology has its background in drag reduction on trans- and super-sonic wings. Drag reduction is achieved by placing a thin cavity with porous surface where the shock wave is located. The higher pressure behind the shockwave circulates the air through the cavity to the lower pressure ahead of the shock. This effects both boundary-layer separation and entropy in a positive way.

The techniques tested are described in figure 29 b. A fully porous surface has little or no positive effect on the pressure distribution. But a non-porous surface separating a porous surface downstream and tangential blowing slot upstream has some positive on pressure distribution as illustrated by figure 32.

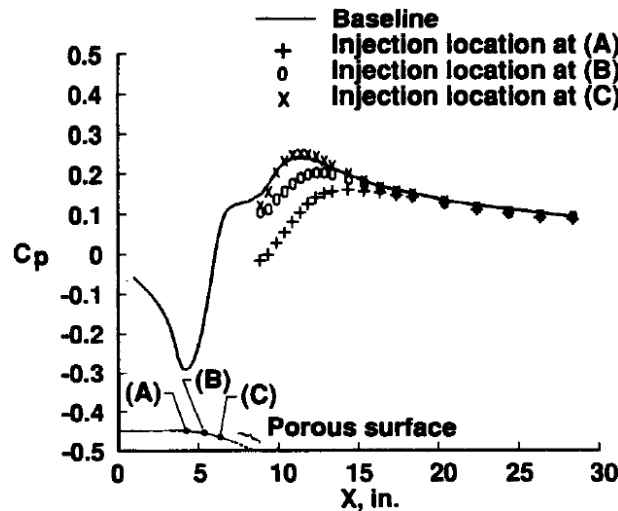


Figure 32: Pressure distribution for passive tangential blowing. [13]

The most beneficial configuration is when the 0.8 mm (0.032-inch) tangential gap is placed at the baseline separation location (location C in figure 32). The problems with the technique (pressure driven self-bleeding) are probably due to insufficient mass flow but the technology might have applications for more severely separated cases with larger adverse pressure gradients.

3.3. Vortex generators

Vortex generators have normally been used to increase low speed, high angle performance on aircraft and to reattach separated flow on airfoils. On a flap deflection of 35° Lin et. al. [14] managed to reattach the airflow completely.

Wheeler vortex generators have in commercial tests within the trucking industry [13] indicated up to 10 % fuel mileage improvement.

When performing tests at the NASA Langley wind tunnel [13], to be able to measure the drag of the vortex generators a balance was used. A Piezoresistive deflection sensor was used to convert displacement into drag force. The range of the balance was 0 – 8.9 kPa (0 – 1.3 lbf) with a resolution of 1.5 Pa ($2.2 \cdot 10^{-4}$ lbf.) The measurement of the drag was conducted with vortex generators placed 152 mm (6 inches) and 1067 mm (42 inches) upstream of the separation ramp described in figure 24.

3.3.1. Vane-type vortex generators

One-inch-high vane-type counter rotating vortex generators as described by figure 29 d was initially tested and it provided attached flow directly downstream the generators. When moved from 5δ (16 cm) to 15δ (49 cm) upstream of the baseline separation line the generators maintained their efficiency. Figure 33 show three spanwise pressure distributions at 0, $\lambda/4$ and $\lambda/2$ distance away from the device centreline.

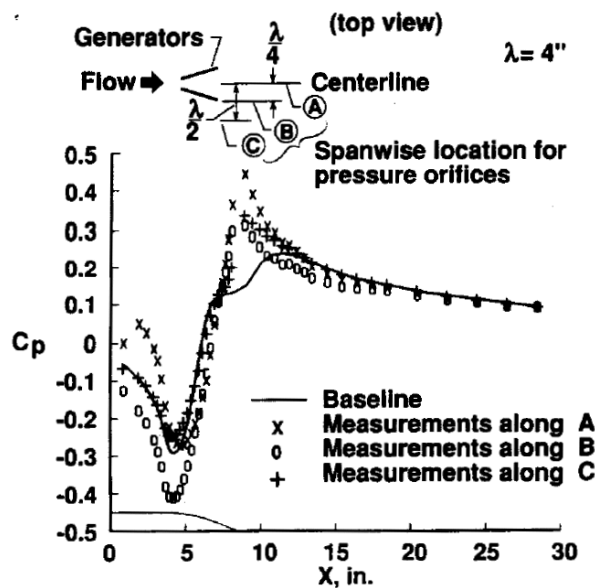


Figure 33: Pressure distribution for 1-inch-high counter-rotating vortex generators at $5d$ upstream of the baseline separation. [13]

Figure 33 also show an improved pressure recovery but also a reduction of pressure on ramps shoulder region. This is desirable if one wants to increase lift but result in a pressure drag penalty. The reduction in pressure is caused by increase in local velocity resulting from the redirection of high momentum airflow from outer parts of boundary layer.

3.3.2. Wheeler vortex generators

The configuration with Wheeler generators is illustrated by figure 29 d.

Flow visualisations for the Wheeler vortex generators show that the optimal placement is just ahead of the horizontal tangential location on the shoulder of the separation ramp. Oil flow visualisations indicate that both 12,5- and 3- mm ($\frac{1}{2}$ - and $\frac{1}{8}$ - inch) high generators, when placed at the optimum location, are efficient and reduce reattachment distance up to 66 %.

Figure 34 a and b show pressure distributions for different spanwise location of pressure taps. Figure 34 a for the 12,5 mm high generators and figure 34 b for the 3 mm high generators. The variations are much smaller than for the vane-type generators and the 3 mm Wheeler generators produce virtually no difference in pressure distribution spanwise.

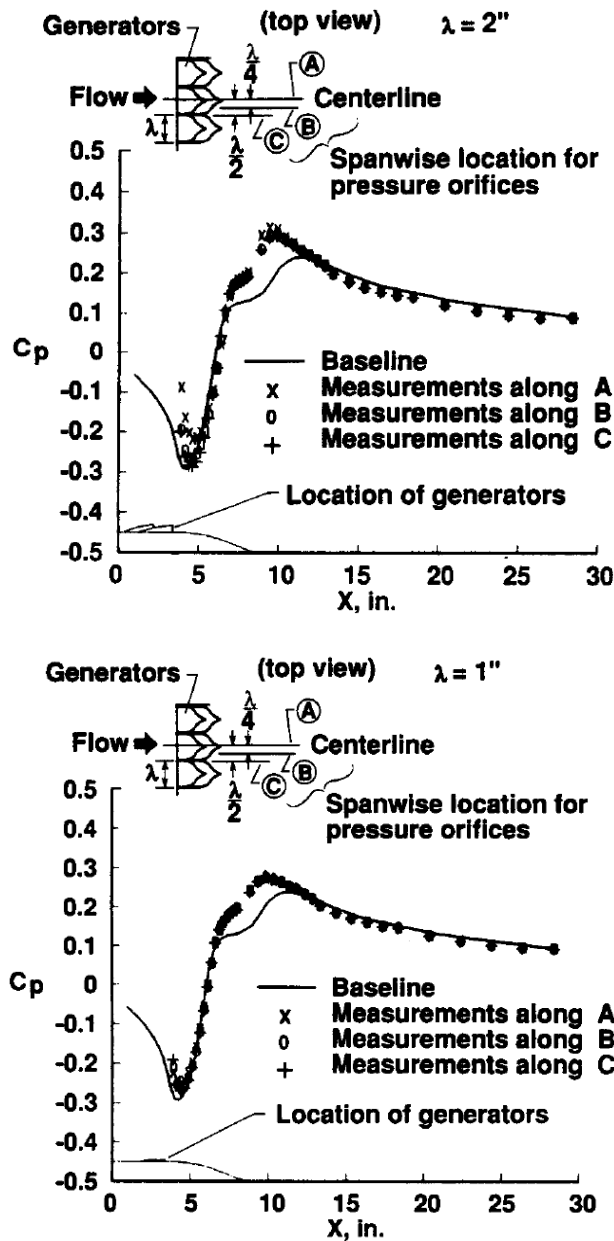


Figure 34(a-b): Pressure distributions for Wheeler vortex generators. [13]

Since the Wheeler vortex generators produce less three-dimensional flow, indicated by the lack of variation in pressure distribution spanwise, it minimise pressure reduction at the shoulder of the ramp and thus is more beneficial for pressure-drag reduction.

The beneficial behaviour of the low Wheeler generators is because the turbulent velocity profile of the boundary layer as described by figure 35.

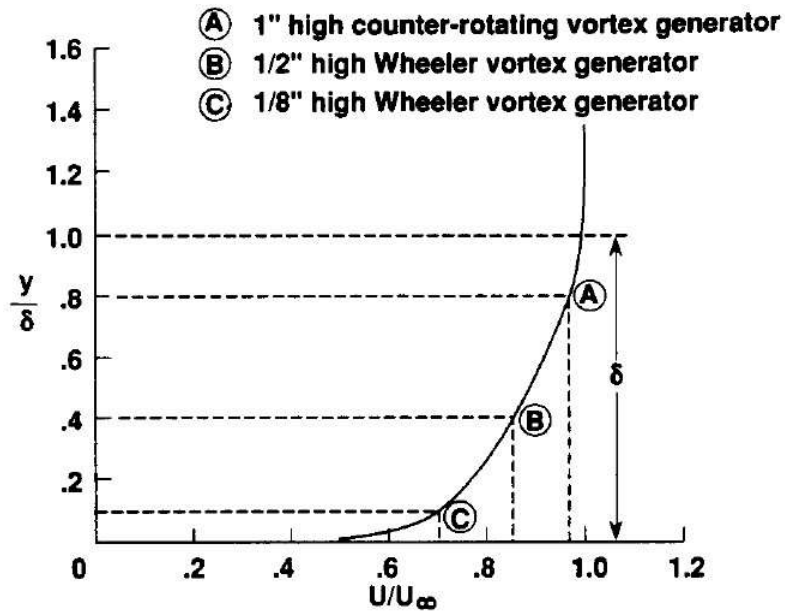
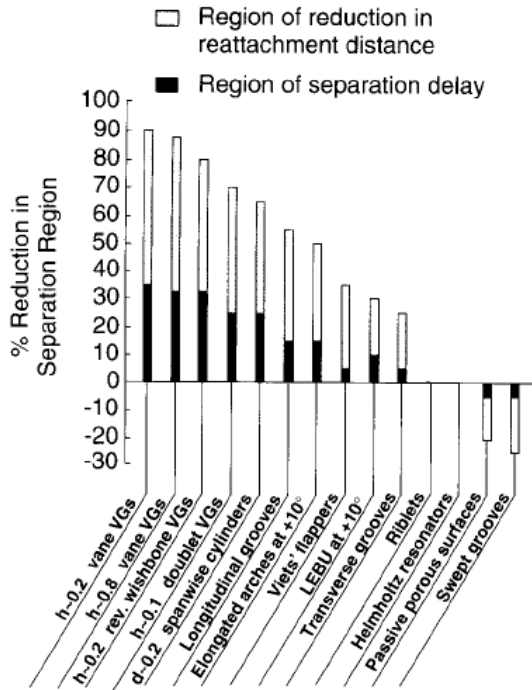


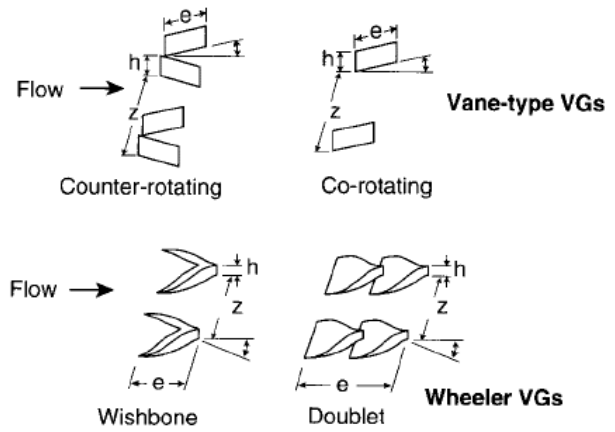
Figure 35: Location height to boundary layer profile. [13]

At device heights of 0.2δ the local velocity is over 75 % of the free-stream value and further increase in height only give minor addition to air speed.

J.C. Lin summarised the results [15] in figure 36 and illustrate the baseline configuration separation compared to the configurations with VG using oilflow as shown in figure 37 a-c.

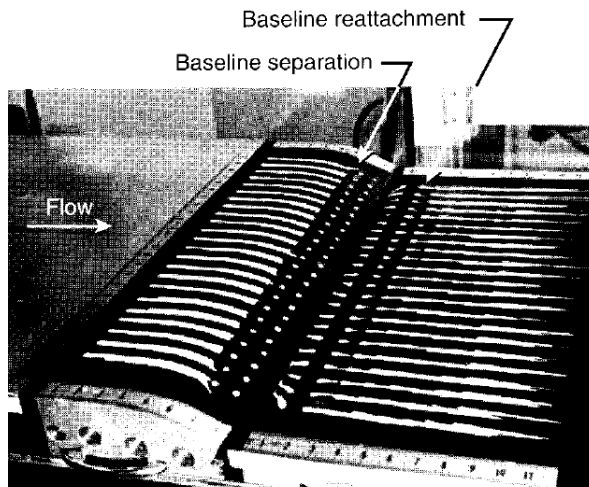


(a) Summary: relative effectiveness in flow separation control versus device category.

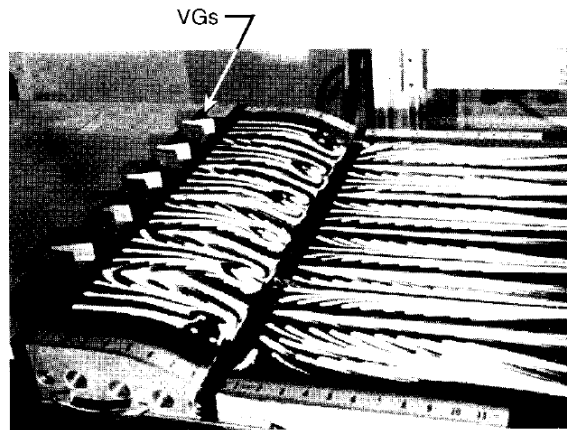


(b) VG geometry and device parameters.

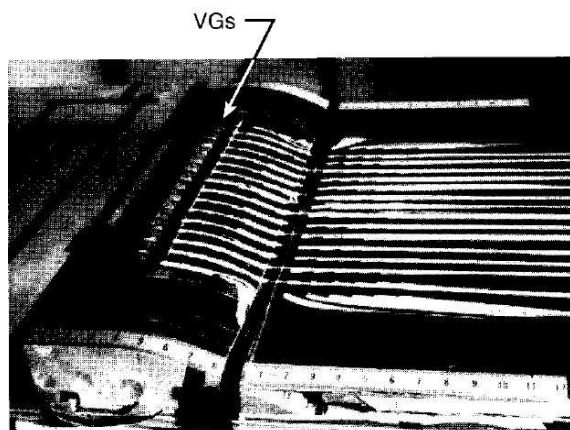
Figure 36(a-b): Relative effectiveness in flow separation control versus device category. [15]



(a) Baseline (VG off) case.



(b) 0.8δ -high vane-type counter-rotating VGs at $6h$ upstream of baseline separation.



(c) 0.2δ -high vane-type counter-rotating VGs at $10h$ upstream of baseline separation.

Figure 37(a-c): Oil-flow demonstrating the effect of different configurations. a) The baseline configuration. b) 0.8δ -high vane-type counter-rotating VGs at $6h$ upstream of baseline separation. c) 0.2δ -high vane-type counter-rotating VGs at $10h$ upstream of boundary layer. [15]

The most effective range using low-profile VGs would be at $5 - 30h$ upstream baseline separation although the vortices could last up to $100h$. The most efficient device height seems to be somewhere within $0.2 - 0.5h/\delta$ since using a device of $0.1h/\delta$ or less reduce the effectiveness of the devices. Vane-type VGs is preferred before Wishbone or Wheeler VGs since for an equal amount of vorticity vane-type VGs produce less drag.

These results coincide with the results retrieved by Kristian Angele [16] who present results that suggest that the vortices are fully developed $9 - 13$ boundary layers downstream of the VGs as presented in figure 38. Angele set up an experiment with vane-type VGs using design criteria suggested by Pearcey and defined in table 7. The experiment was set up in an adverse pressure gradient (APG) and turbulent boundary layer was generated by rows of Dymo-tape as tripping device. Measurements were conducted at a Reynolds number of $9.2 \cdot 10^6/m$ based on inlet airflow of 14 m/s . Counter-rotating vortices was used since they are more efficient than the co-rotating ones for 2D cases, although Lin [15] suggest co-rotating VGs for 3D cases.

Using particle imaging velocity (PIV) the behaviour of the vortices behind the VGs were registered at three different locations behind the VGs: $x/h = 5.5, 9$ and 13 , that result in figures

38 a-f. They confirm the statements that a fully energized boundary layer takes some 15 boundary layers downstream the VGs to fully develop.

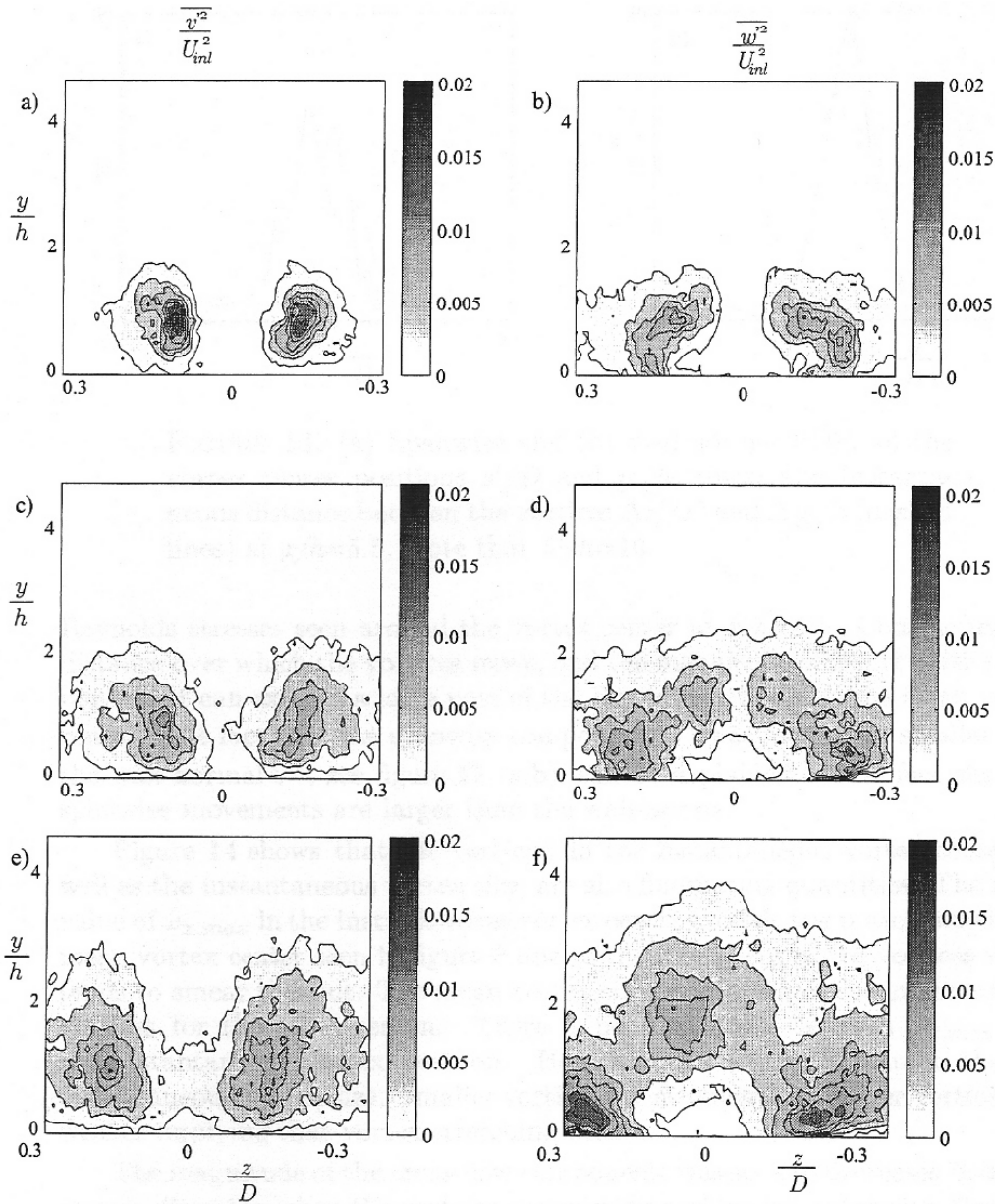


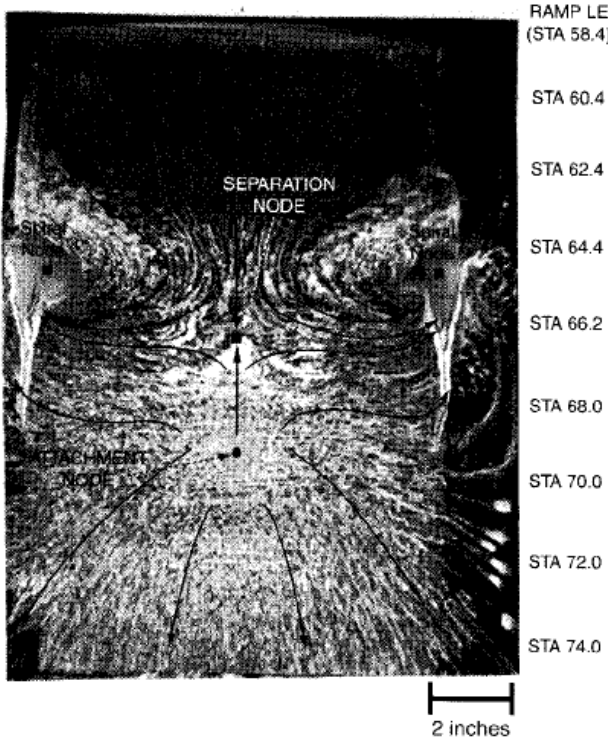
Figure 38(a-f): Secondary flow components generated by VGs in the yz-plane (perpendicular to the general airflow direction). a-b) $x/h = 5.5$ c-d) $x/h = 9$ e-f) $x/h = 13$. v^2 and w^2 are the different crossflow components in the yz-plane. [16]

l	h	d	δ	β
30 mm	10 mm	25 mm	10 mm	15°

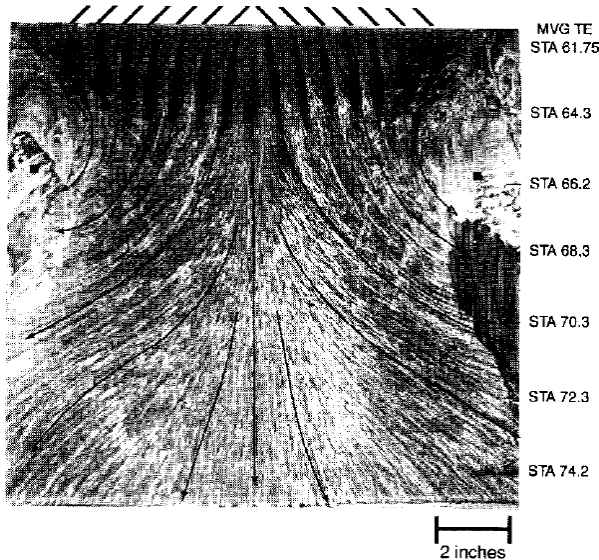
Table 7: Definition of experimental set up by K. Angele. [16]

Low-profile VGs probably need a further distance to develop since they interact with a smaller part of the boundary layer than the boundary layer sized VGs used in the K. Angele experiments.

Another successful attempt to use low-profile VGs is presented on the flow over a backward facing ramp dominated by a 3D separated flow generated by two large junction vortices – one over each side-corner of the ramp. Figure 39 a show the large spiral nodes at the ramps side edges and the reverse flow at the centre of the ramp.



(a) Baseline (VG off) case.



(b) 0.2δ-high vane-type co-rotating VGs at 12 h upstream of baseline separation.

Figure 39(a-b): Oil flow visualizations on the effect of using VGs to reduce 3D flow over a backward-facing ramp. [15]

Figure 39 b show how low-profile VGs ($h/\delta = 0.2$, $e/h = 4$, $\Delta z/h=4$, $\beta= 23^\circ$, airspeed 42.7 m/s (140 ft/s)) efficiently reduce the flow separation and the flow in the centre of the ramp

maintain attached. Further investigation also suggests that there is no major difference in effectiveness of the low-profile VGs when placed somewhere $20 h$ upstream of baseline configuration separation.

3.3.3. Blunt body application of Vortex Generators

W. Calarese et. al. [17] performed a series of experiments on the effect of vortex generators on total drag of a 1/72 scale model of a C-130 aircraft. The model was selected because of its highly up-swept afterbody that generate a high adverse pressure gradient and the wish from its operators (US Airforce) to reduce its fuel consumption.

Tests were performed at Air Force Institute of Technology. Their wind tunnel is an open return, closed section tunnel with a circular test section of 1.524 m (5 ft.) in diameter and 5.4864 m (18 ft.) in length. The balance is a 3-component wire balance with accuracy within 0.0002 N (0.02 pound.), 40 pressure taps were placed at the bottom and side of the rear fuselage and on the up-swept afterbody. For placement see figure 40.

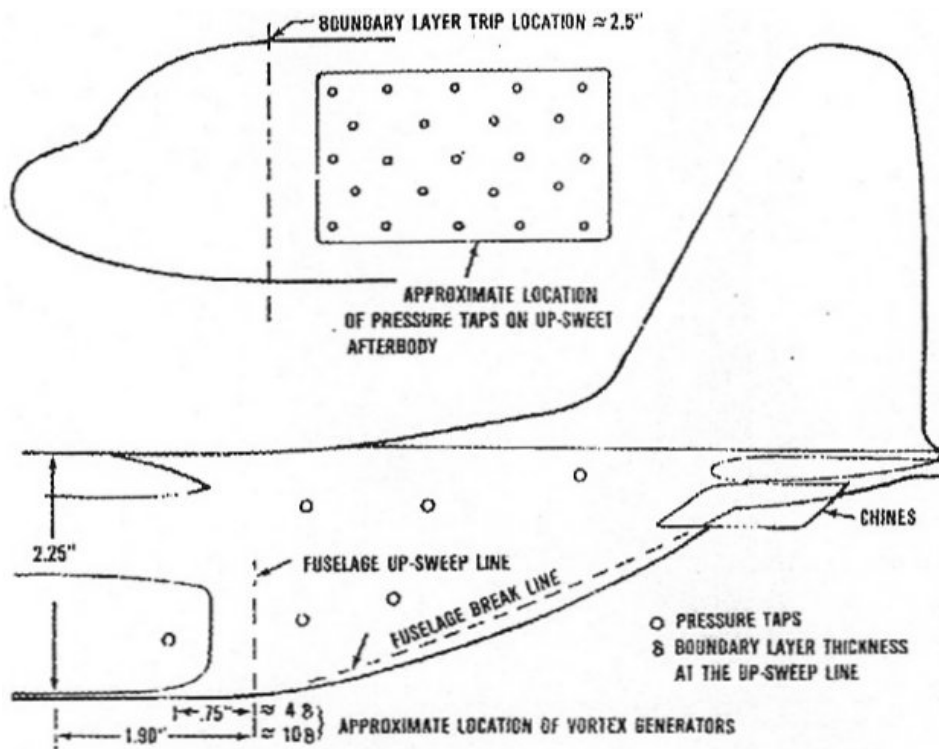


Figure 40: Schematic of pressure taps. [17]

Boundary layer thickness that was defined by the formula of a flat plate in turbulent flow as defined by equation 4.

$$\delta = \frac{0.37 \cdot x_T}{(\text{Re})^{1/5}} \quad (4)$$

The turbulent boundary layer begun at the tripwire illustrated in figure 40 and the distance to the up-sweep line from this location was $x_T = 190 \text{ mm}$ (7.5 inch.) A Reynolds number of $5.78 \cdot 10^5$ resulted in a boundary layer thickness of $\delta = 4.8 \text{ mm}$ (0.19 inch.).

The tests were performed at a Mach number of 0.135 (45 m/s) or a dynamic pressure of 89.3 Pa (60 psf.). All tests were repeated and the data agreed within $\pm 2\%$. The net drag coefficient for the C-130 was measured to a C_d of 0.05 at $\alpha = 0^\circ$. This was consistent with previous data for that model of aircraft.

The two placements of the vortex generators used in tests were 10δ upstream of the afterbody up-sweep line and 4δ upstream the same line as defined in figure 41 with an angle of 16° towards the freestream flow circumferentially around the fuselage. The vortex generators cord was 10.2 mm (0.4 inch) and their span (= device height) was 1.1 times the boundary layer thickness. The trailing edges of the VG were spaced with a distance of 15.2 mm (0.6 inch) as illustrated by figure 41.

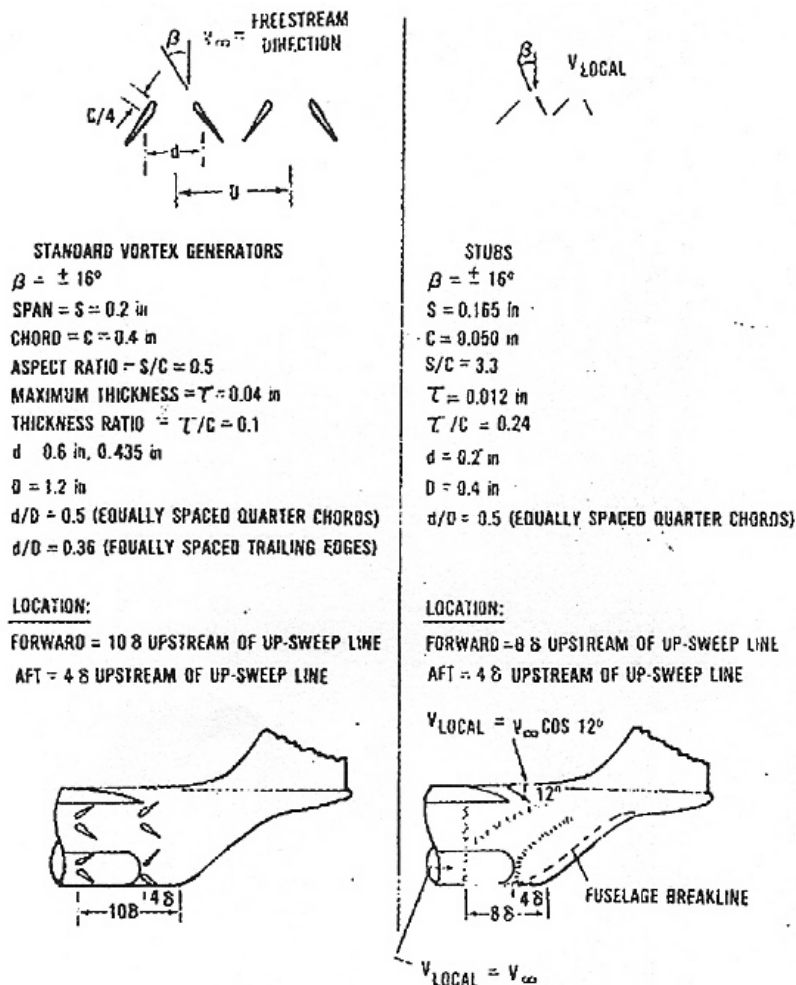


Figure 41: Vortex generators alignment and dimensions. [17]

Another series of tests was performed using small flat stubs with a cord of 1.3 mm (0.05 inch), a span of 4.2 mm (0.165 inch) and a thickness of 0.3 mm (0.012 inch) as defined in figure 41 with an angle of 16° towards the freestream flow. 16 to 22 pairs were used circumferentially around the fuselage and the distance between them were 5 mm (0.2 inch). The “forward” location was 8δ (38 mm) upstream the afterbody up-sweep line and the “aft” location approximately 4δ (19 mm) upstream the same line as defined in figure 41.

The usage of VG resulted in a reduction of the drag coefficient of about 150 counts as demonstrated by figure 42.

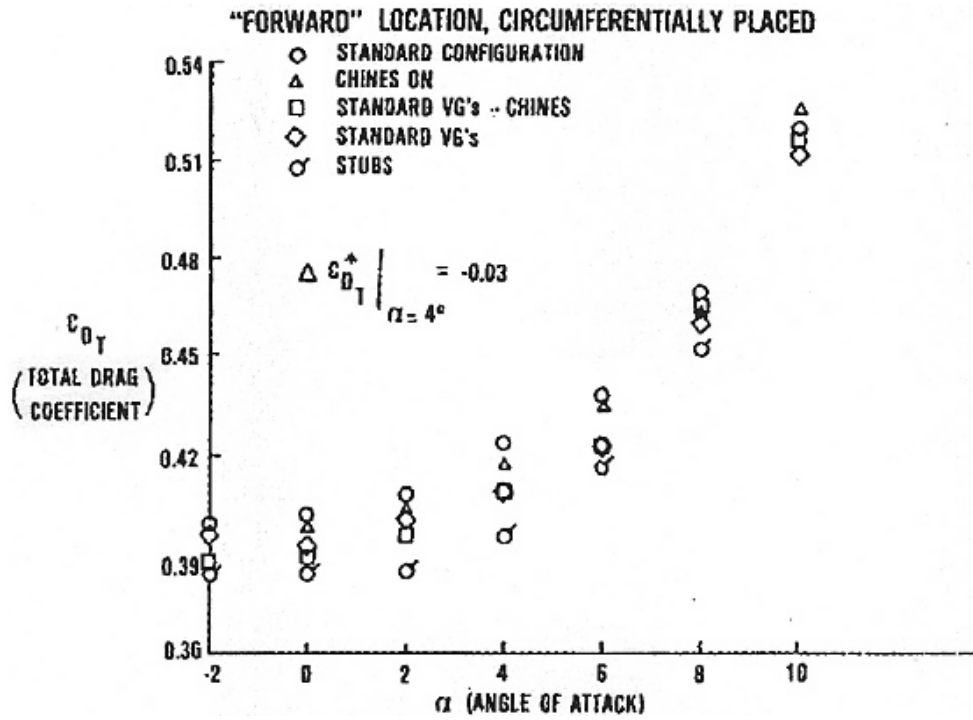


Figure 42: Total drag variation with angle of attack. [17]

But the result for the "stubs" is even better: a reduction of 300 counts is obtained as is shown in figure 43.

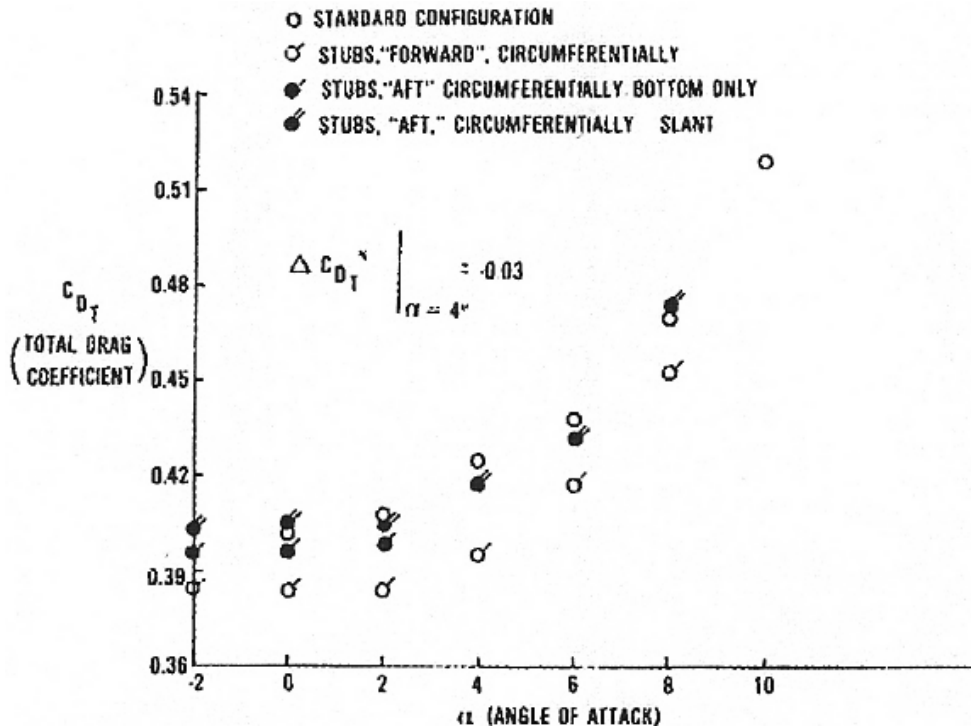
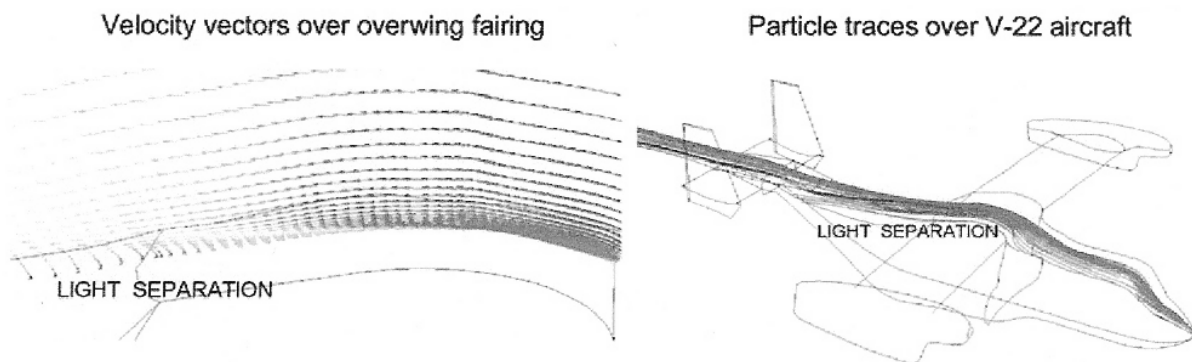


Figure 43: Total drag variation with angle of attack. [17]

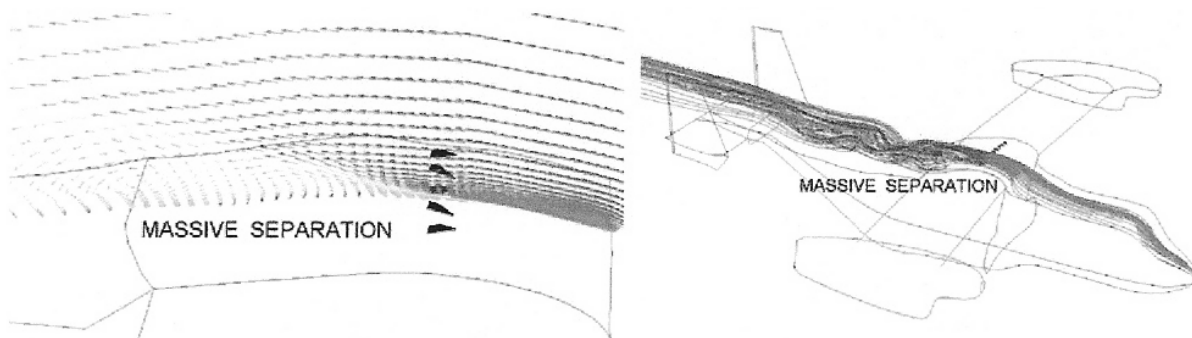
The reduction in drag is more efficient at lower angles of attack and this is beneficial since this corresponds to cruise conditions and this is the condition the aircraft operates at the most of the time. The placement of both the VG and the stubs in the “front” location generated the biggest reductions in drag coefficient. This can be explained by the fact that placement of the VG and stubs on the forward location give the airflow enough time to mix with the freestream flow and thus energize the boundary layer flow, delaying the separation at the up-sweep line.

These results are all in line with those achieved by J.C. Lin et. al. [15] and show the potential of using sub-boundary layer vortex generators in reducing bluff body drag. The smaller device heights give a smaller device drag but give enough energizing of the boundary layer if carefully placed.

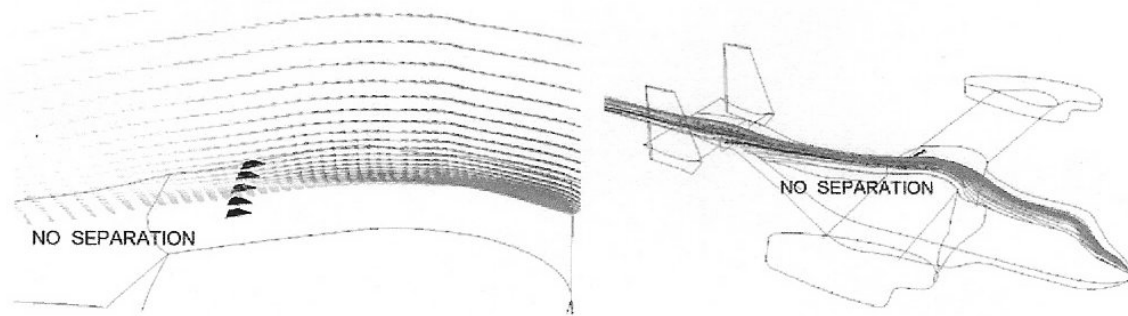
Based on the results in [15] and [16] it is easy to believe that it is beneficial to place VGs as far upstream as possible. But Lin [15] also shows that placement too far upstream can increase flow separation and drag. The Naval Surface Warfare Centre performed some CFD calculations on the overwing fairing of a V-22 aircraft simulating ten low-profile VGs. Figure 44 a illustrate a cruise angle of 7° and light separation. In figure 44 b the placement too far upstream (or too large VGs) of the VGs generate increased separation. By moving the generators 10 device heights downstream the baseline separation (figure 44 c) is eliminated.



(a) VG off baseline (Configuration A).



(b) 10 VGs with $\beta = \pm 20$ deg. located at $\sim 32 h$ upstream of baseline separation (Configuration B).



(c) 10 VGs with $\beta = \pm 9$ deg. located $\sim 10 h$ upstream of baseline separation (Configuration E).

Figure 44(a-c): Velocity vectors over a V-22 overwing fairing. a) no VGs b) $h/d = 1$ c) $h/d = 0.5$ [16]

4. Continued work

Further investigations has been done in the areas of boundary layer control but has not been accounted for in this report. An alternative approach that could be used is the use of sound waves to control the boundary layer separation as suggested by A. Nishizawa and S. Takagi [18].

One of the most interesting areas would be the use of air jets to form vortex generators as suggested by H. Abe et. al. [19]. The benefit with that technology is that it would be possible to control the strength of the jets and thus control the strength of the vortices created. This could translate into different grade of flow attachment at different flow situations and most beneficial of all is the possibility to shut them down and in that case they do not in any way contribute to the overall drag. The downside of them is the same as for controlling boundary layer with blowing and suction; it requires additional equipment for generating the airflows and some kind of control mechanism. That adds cost and complexity to the construction and that is never a good thing in terms of maintenance and cost.

5. Conclusions

Mentionable is that there are measures that are more important to take than changing the airflow around the rear of a vehicle. Those measures are the rounding of front corners which can contribute to as much as 52% drag reduction [6] and a full-length underbody seal can contribute to as much as 15% drag reduction [6]. These measures need to be taken care of before it is interesting to take a look at rear end flow. But when at least the first measure has been taken care of it can be beneficial to take a look at altering rear end airflow.

Based on the results given in [13] and [15] I believe that the most efficient way to reduce base-drag on blunt bodies (such as busses and trucks) is the use of VGs in some way. Preferably low-profile ones to reduce device drag or air-jet VGs that can be turned on and off during different conditions.

One conclusion that can be made from the different reports referred to in this work is that it is difficult to receive the same result in wind-tunnel tests as those received in simulations. This is of course explained by the fact that there are “reality-factors” included in the results received from wind-tunnel tests. That is imperfections in manufacturing of the model, leakage and general losses that is not accounted for in CFD modelling.

Some of the results are gathered in table 8.

Technology	Type of improvement
Boat-tailing	32 % reduction in C_d .
Aerodynamic boat-tail	10 % reduction in C_d .
Blown boundary layers at GTRI	50 % reduction in C_d . *
CFD, round rear edge	14 % reduction in C_d .
CFD, round rear edge, suction of bl**	24 % reduction in C_d .
Wind-tunnel test, boat-tail, blowing of bl**	12 % reduction in C_d .
Transversal grooves on a shoulder	20 % shorter distance to reattachment
Longitudinal grooves on a shoulder	66 % shorter distance to reattachment
Angled grooves on a shoulder	Not conclusive ***
Passive porous surface	Some improvement
Micro vortex generators	300 counts

Table 8: Summary of some of the results presented in the report. *=compared to no aerodynamic optimisation at all = sharp front end, no fairing. **bl=boundary layer. *= [12] suggest a 50 % drag reduction**

Judging from these results it seems like blowing boundary layers would be the most beneficial way to reduce rear end drag. But in this case, and several others, there is the “reality factor” to consider as mentioned above in this section, tests performed at GTRI was performed on an “ideal body” and can not be easily be compared to other results.

Then there is the traditional boat-tailing that come in second. These results are more reliable since they are performed on a real vehicle, still it is ideal in many ways but they give a hint of what kind of results we want to achieve. And as I mentioned earlier they can be used as a bench mark for other tests since they present the most ideal flow case (a full boat-tail) but with some separation so that result can be somewhat improved. Results much better than this (for example the GTRI result) should be seen upon with some scepticism before presented to others. Or at least thoroughly explained why that kind of result is received.

So in real life, what seems to be the best technology to apply to your vehicles? With little or no difference in manufacturing technology rounding of the rear edges seems so far to be the best way as for now to receive smaller contribution to the overall drag. In combination with grooves could improve the pressure recovery mechanism at the rear of blunt vehicles and with proper placement and design I believe that VGs in some kind belong to future design of high performing commercial vehicles.

6. References

- [1] Wolf-Heinrich Hucho; Aerodynamics of Road Vehicles, ISBN 0-7680-0029-7
- [2] Alfons Gilhaus; The main parameters determining the aerodynamic drag of buses, Neue Technologie, M.A.N. München, June 1981
- [3] Edwin J. Saltzman; A summary of NASA Dryden's Truck Aerodynamic Research, SAE Technical Paper Series, 821284
- [4] Robert D. Blevins; Applied fluid dynamics handbook, ISBN 0-442-21296-8
- [5] Randall L. Peterson; Drag reduction by the addition of a boat-tail to a box shaped vehicle, NASA Contractor Report 163113, August 1981
- [6] Robert J. Englar; Development of Pneumatic Aerodynamic Devices to Improve the Performance, Economics, and Safety of Heavy Vehicles. SAE Paper 2000-01-2208. June 19-21, 2000
- [7] Robert J. Englar; Advanced Aerodynamic Devices to Improve the Performance, Economics, Handling and Safety of Heavy Vehicles. SAE Paper 2001-01-2072. May 14-16, 2001
- [8] B.S. Massey, Mechanics of Fluids, sixth edition, ISBN 0-412-34-280-4
- [9] Paola Ferraresi; Control of Boundary Layer Flow on Trucks. Master Thesis, Skrift 2001-14. Department of Aeronautics, Royal Institute of Technology, SE-100 44 Stockholm, Sweden
- [10] Benjamin Le Roux; Experimental Aerodynamics: Separation Control on Trailers of Trucks, A Master Thesis at Scania CV AB, RTTF section. May 2003
- [11] Wendy R. Lanser, James C. Ross and Andrew E. Kaufman; Aerodynamic Performance of a Drag Reduction Device on a Full-Scale Tractor/Trailer, SAE Paper 912125
- [12] G.V. Selby, J.C. Lin and F.G. Howard. Turbulent flow separation control over a backward-facing ramp via transverse and swept grooves. Journal of Fluids Engineering, June 1990, Vol. 112
- [13] J. C. Lin and F. G. Howard, Turbulent Flow Separation Control Through Passive Techniques. NASA Langley Research Center, Hampton, VA; and G.V. Selby, Old Dominion University, Norfolk, VA. AIAA 89-0976. March 13-16, 1989
- [14] S. Klausmeyer, M. Papadakis, J. Lin; A Flow Physics Study of Vortex Generators on a Multi-Element Airfoil, AIAA 96-0548
- [15] John C. Lin; Review of research on low-profile vortex generators to control boundary-layer separation. Progress in Aerospace Sciences 38 (2002) 389-420.
- [16] Kristian Angele; Experimental studies of turbulent boundary layer separation and control. Royal Institute of Technology, Department of Mechanics. Technical report 2003:08. ISSN 0348-467X
- [17] W. Calarese, W.P. Crisler and G.L. Gustafson; Afterbody Drag Reduction by Vortex Generators, Flight Dynamics Laboratory, Air Force Wright Aeronautical Laboratories, Wright_Patterson Air Force base, Ohio. AIAA-85-0354. January 14-17, 1985/ Reno, Nevada
- [18] Akira Nishizawa, Shohei Takagi; Toward smart control of separation around a wing – Development of an Active Separation Control System, National Aerospace Laboratory of Japan, Chofu, Tokyo, 182-8522
- [19] Hiroyuki Abe, Takehiko Segawa, Takayuki Matsunuma, Hiro Yoshida; Management of a Longitudinal Vortex for Separation Control, National Institute of Advanced Industrial Science and Technology, Japan